A&A 525, A60 (2011)
DOI: 10.1051/0004-6361/201015499

Astronomy & Astrophysics

Time damping of non-adiabatic magnetohydrodynamic waves in a partially ionised prominence medium: Effect of a background flow

S. Barceló[1], M. Carbonell[2], and J. L. Ballester[1]

[1] Departament de Física, Universitat de les Illes Balears, 07122 Palma de Mallorca, Spain
[2] Departament de Matemàtiques i Informàtica, Universitat de les Illes Balears, 07122 Palma de Mallorca, Spain
e-mail: [s.barcelo;marc.carbonell;joseluis.ballester]@uib.es

Received 29 July 2010 / Accepted 9 October 2010

ABSTRACT

Context. The simultaneous occurrence of flows and time damped small-amplitude oscillations in solar prominences is a common phenomenon. These oscillations are mostly interpreted in terms of magnetohydrodynamic (MHD) waves.
Aims. We study the time damping of linear non-adiabatic MHD waves in a flowing partially ionised plasma with prominence-like physical conditions.
Methods. Considering non-adiabatic single fluid equations for a partially ionised hydrogen plasma, we have solved our dispersion relations for the complex frequency, ω, and we have analysed the behavior of the period, damping time and the ratio of the damping time to the period, versus the real wavenumber k, for Alfvén, fast, slow, and thermal waves.
Results. While in the case without flow there is a critical wavenumber at which the period of Alfvén and fast waves goes to infinite, when a flow is present two different critical wavenumbers appear. The smaller wavenumber depends on the flow speed and causes the period of the high-period branch to go to infinite. When the second critical wavenumber is attained the period of both branches become equal. In general, the time damping of Alfvén and fast waves is dominated by resistive effects, and its damping ratio is very inefficient when compared to observations. The damping of slow and thermal waves is basically dominated by non-adiabatic effects, and for slow waves it is possible to obtain a damping ratio close to observations, although it would correspond to long period oscillations with large damping times not often observed. The consideration of a structured medium produces new features such as the apparition of four critical wavenumbers for Alfvén waves, and one critical wavenumber for slow waves. For fast waves, constrained propagation substantially improves, within the range of observed wavelengths, the ratio of the damping time to period.
Conclusions. The presence of a background flow in a partially ionised plasma gives place to new interesting features when the time damping of MHD waves is studied. In general, the results point out that ion-neutral collisions are an inefficient mechanism to explain the observed time damping of prominence oscillations if they are produced by Alfvén and fast waves. If the oscillations are produced by slow waves, only long period oscillations with large damping times produce damping ratios in agreement with observations.

Key words. Sun: oscillations – Sun: filaments, prominences

1. Introduction

Quiescent solar prominences are usually thought to be cool ($T \sim 10^4$ K) and dense ($\rho \sim 5 \times 10^{-11}$ kg/m^3) plasma clouds located in the much denser and hotter solar corona. It is still a matter of debate how these dense and cool structures live for a long time within the solar corona, although a widely extended idea is that its support and thermal isolation are of magnetic origin. On the other hand, the typical composition of solar prominences is 90% hydrogen and 10% helium, but its exact ionisation degree is unknown (Labrosse et al. 2010) and the ratio of electron density to neutral hydrogen density seems to be in the interval 0.1−10 (Patsourakos & Vial 2002). Therefore, solar prominences seem to be made of partially ionised plasmas and hydrogen lines are routinely observed (Labrosse et al. 2010).

Solar prominences usually display two important features: oscillations and flows. Using ground and space-based observations, small-amplitude oscillations in prominences and filaments have been observed and details about their properties can be found in Oliver & Ballester (2002), Banerjee et al. (2007), Oliver (2009), and Mackay et al. (2010). These oscillations are mainly detected by the periodic Doppler shifts of spectral lines, with periods from a few minutes to hours, and one interesting feature is that they are damped in time.

Observational evidence of the time damping of small amplitude oscillations in prominences has been reported by Landman (1977), Tsubaki & Takeuchi (1986), Tsubaki (1988), Wiehr et al. (1989), Molowny-Horas et al. (1999), Terradas et al. (2002), Lin (2004), Berger et al. (2008) and Ning et al. (2009a,b). Molowny-Horas et al. (1999) and Terradas et al. (2002) studied two-dimensional time series from a quiescent prominence and found that oscillations detected in large areas of the prominence were typically damped after 2−3 periods. Similar results have been obtained recently by Mashnich et al. (2009). The same behavior is found in high-resolution Doppler time series from individual filaments threads (Lin 2004) and in *Hinode*/SOT observations by Ning et al. (2009a) who reported a maximum number of 8 periods before the oscillations disappeared. More extense reviews about the damping of small-amplitude prominence oscillations

can be found in Oliver (2009), Ballester (2010) and Arregui & Ballester (2010).

Flows are a typical characteristic of prominences and have been observed in Hα, UV, and EUV lines (Labrosse et al. 2010). In Hα quiescent filaments, the observed velocities range from 5 to 20 km s^{-1} (Zirker et al. 1998; Lin et al. 2003, 2005, 2007; Schmieder et al. 2008; Chae et al. 2006; Labrosse et al. 2010) and, because of the physical conditions in filament plasma, they seem to be field-aligned. Also, the presence in filaments of oscillating absorbing features which, at the same time, move along the filament axis has been reported (Lin 2004). In limb prominences different kinds of flows are observed (Chae et al. 2008; Schmieder et al. 2010) and, for instance, observations made by Berger et al. (2008) with *Hinode*/SOT pointed out a complex dynamics with vertical downflows and upflows. In this case, velocities seem to be slightly higher than in filaments (up to 35 km s^{-1}) and the orientation with respect to the magnetic field is unclear (Chae et al. 2008; Schmieder et al. 2010; Labrosse et al. 2010). Finally, in active region prominences flow speeds can be higher (Okamoto et al. 2007)

Related with flows and oscillations interpreted in terms of MHD waves, we would like to point out that while from a theoretical point of view we know how to deal with flows and waves, from an observational point of view it can be quite difficult. For a proper interpretation of the observations, it is very important to be able to distinguish between both features and, nowadays, and in the framework of coronal physics, a lively discussion is going on about how to discriminate between flows and waves in the observations of quasi-periodic phenomena in solar coronal structures. Up to now, no agreement has been reached yet. The same observations about quasi-periodic and propagating intensity perturbations or quasi-periodic propagating signals have been interpreted as slow magnetoacoustic waves or as upflows. It seems that unequivocal identification can only be done in particular cases. For instance, Jess et al. (2009) reported the detection of oscillatory features associated with a large bright point group. The observations did not show evidence of transversal displacements and intensity oscillations, which discarded an interpretation in terms of magnetoacoustic waves but allowed a probable interpretation in terms of Alfvén waves.

Usually, small-amplitude prominence oscillations are interpreted in terms of linear magnetohydrodynamic (MHD) waves and their damping has been studied by considering different wave dissipative mechanisms. For instance, for fully ionised plasmas, the time damping of prominence oscillations has been studied by considering non-adiabatic MHD waves, including the effects of optically thin radiation, thermal conduction, and heating, in unbounded and bounded prominence slabs (Carbonell et al. 2004; Terradas et al. 2005), prominence slabs surrounded by an infinite solar corona (Soler et al. 2007) and bounded prominence-corona slabs (Soler et al. 2009c). On the other hand, taking into account the fine prominence structure, and assuming that the threads forming solar filaments can be modeled as cylindrical flux tubes filled with fully ionised prominence plasma surrounded by the solar corona, the time damping of inhomogeneous cylindrical flux tubes due to resonant absorption has been studied by Arregui et al. (2008).

The effect of partial ionisation was considered by Mercier & Heyvaerts (1977) when they studied the difusion of neutral atoms by gravity. Gilbert et al. (2002) studied the diffusion of neutral atoms in a partially ionised prominence plasma, concluding that the loss timescale is much longer for hydrogen than for helium. Gilbert et al. (2007) investigated the temporal and spatial variations in the relative abundance of helium with respect to hydrogen in a sample of filaments. They found that a majority of filaments show a deficit of helium in the top part, while in the bottom part there is an excess. This seems to be due to the shorter loss timescale of neutral helium compared to that of neutral hydrogen. The consideration of prominences as partially ionised plasma is extremely important for the physics of prominences, and the effects on MHD waves in prominences need to be taken into account. From the theoretical point of view, and related with laboratory plasma physics, there is an extensive amount of literature about wave propagation in a partially ionised multifluid plasma (Watanabe 1961a,b; Tanenbaum 1961; Tanenbaum & Mintzer 1962; Woods 1962; Kulsrud & Pearce 1969; Watts & Hanna 2004). In astrophysical plasmas, the typical frequency of MHD waves is much lower than the collisional frequencies between species. In this case, the single fluid approach is usually adopted and has been applied to wave damping in the solar atmosphere (De Pontieu et al. 2001; Khodachenko et al. 2004; Leake et al. 2005). In the case of solar prominences, Forteza et al. (2007) derived the full set of MHD equations for a partially ionised, single-fluid plasma and applied them to study the time damping of linear, adiabatic waves in an unbounded prominence medium. This study was later extended to the non-adiabatic case by including thermal conduction by neutrals and electrons, radiative losses, and heating (Forteza et al. 2008). Because of the effect of neutrals, in particular that of ion-neutral collisions, a generalized Ohm's law has to be considered, which causes some additional terms to appear in the resistive magnetic induction equation relative to the fully ionised case. Among these additional terms, the dominant one in the linear regime is the so-called ambipolar magnetic diffusion, which enhances magnetic diffusion across magnetic field lines. Furthermore, one of the interesting effects produced by the consideration of partial ionisation and ion-neutral collisions is that Alfvén waves can be damped, which cannot be obtained by means of thermal mechanisms, and Singh & Krishnan (2009) studied the time damping of Alfvén-like waves in a partially ionised plasma representing a particular model of the solar atmosphere. For bounded media, Soler et al. (2009d) applied this formalism to the study of the time damping of fast, Alfvén, and slow waves in a partially ionised filament thread modeled as a cylinder, and Soler et al. (2009b,e) used a cylindrical filament thread, having an inhomogeneous transition layer between prominence and coronal material, to study the influence of partial ionisation on the time damping of fast kink waves caused by resonant absorption in the inhomogeneous layer. Finally, Soler et al. (2010) have explored the influence of helium in the attenuation of oscillations by ion-neutral collisions obtaining that under prominence conditions is completely negligible.

Taking flows into account, Carbonell et al. (2009) explored the time damping of non-adiabatic slow and thermal waves in an unbounded and fully ionised prominence medium with a background flow, while Soler et al. (2008, 2009a) investigated the time damping of the oscillations of an individual prominence thread and of a threaded prominence when both mass flows and non-adiabatic processes are considered. However, it remains to be explored the effect produced by the joint action of flows and non-adiabatic processes in partially ionised plasmas in the propagation and attenuation of MHD waves responsible for prominence oscillations. Therefore, our main aim here is to explore the theoretical and observational effects associated with the time damping of non-adiabatic MHD waves in an unbounded and partially ionised plasma, with prominence-like physical conditions, when a background flow is present. The layout of the paper is as follows: in Sect. 2, the equilibrium model and some theoretical

considerations are presented; in Sects. 3 and 4, the time damping of Alfvén and magnetoacoustic waves in an unbounded prominence medium is studied; in Sect. 5, the effect of magnetic structure is taken into account; finally, in Sect. 6, our conclusions are drawn.

2. Model and methods

2.1. Equilibrium properties

As a background model, we use a homogeneous unbounded medium threaded by a uniform magnetic field along the x-direction, and with a field-aligned background flow. The equilibrium magnitudes of the medium are given by

$$p_0 = \text{const.}, \quad \rho_0 = \text{const.}, \quad T_0 = \text{const.},$$

$$\boldsymbol{B}_0 = B_0\hat{\boldsymbol{x}}, \quad \boldsymbol{v}_0 = v_0\hat{\boldsymbol{x}},$$

where B_0 and v_0 are constants, and the effect of gravity has been ignored. Since we consider a medium with physical properties akin to those of a quiescent solar prominence, the density is $\rho_0 = 5\times10^{-11}$ kg/m^3, the temperature $T_0 = 8000$ K, and the magnetic field $|\boldsymbol{B}_0| = 10$ G, and we consider a field-aligned flow with $v_0 = 15$ km s^{-1}, simulating the typical flows observed in quiescent filaments. However, a smaller value, $v_0 = 10$ km s^{-1}, has been also considered to highlight some features which can appear in slow waves.

2.2. Basic and linearised equations

Single-fluid MHD equations for a partially ionised hydrogen plasma were derived in Forteza et al. (2007), and later were extended by including terms representing non-adiabatic processes in the energy equation (Forteza et al. 2008). The physical meaning of all the terms and quantities used in the following can be found in those papers. When a background flow is considered, the single fluid basic equations for the study of non-adiabatic MHD waves in a partially ionised plasma can be derived from Forteza et al. (2007, 2008) and Carbonell et al. (2009). The most important difference with respect to the non-adiabatic case without a background flow is that instead of the operator $\frac{\partial}{\partial t}$, we have $\frac{\partial}{\partial t} + \boldsymbol{v}_0\cdot\nabla$ in the MHD equations (Goedbloed & Poedts 2004).

We consider a partially ionised hydrogen plasma characterized by a plasma density, ρ_0, temperature, T_0, and number densities of neutrals, n_n, ions, n_i, and electrons n_e, with $n_\mathrm{e} = n_\mathrm{i}$. Thus, the gas pressure is $p_0 = (2n_\mathrm{i} + n_\mathrm{n})k_\mathrm{B}T_0$, where k_B is Boltzmann's constant. The relative densities of neutrals, ξ_n, and ions, ξ_i, are given by

$$\xi_\mathrm{n} = \frac{n_\mathrm{n}}{n_\mathrm{i}+n_\mathrm{n}}, \qquad \xi_\mathrm{i} = \frac{n_\mathrm{i}}{n_\mathrm{i}+n_\mathrm{n}}, \tag{1}$$

where we have neglected the contribution of electrons. We can now define a quantity, $\tilde{\mu}$, given by,

$$\tilde{\mu} = \frac{1}{1+\xi_\mathrm{i}}, \tag{2}$$

which gives us information about the plasma degree of ionisation. Following Eq. (2), for a fully ionised plasma $\tilde{\mu} = 0.5$, while for a neutral plasma $\tilde{\mu} = 1$.

The dispersion relation for linear MHD waves has been obtained by considering small perturbations from equilibrium of the form

$$\begin{aligned} \boldsymbol{B}(t,\boldsymbol{r}) &= \boldsymbol{B}_0 + \boldsymbol{B}_1(t,\boldsymbol{r}), & p(t,\boldsymbol{r}) &= p_0 + p_1(t,\boldsymbol{r}),\\ \rho(t,\boldsymbol{r}) &= \rho_0 + \rho_1(t,\boldsymbol{r}), & T(t,\boldsymbol{r}) &= T_0 + T_1(t,\boldsymbol{r}),\\ \boldsymbol{v}(t,\boldsymbol{r}) &= \boldsymbol{v}_0 + \boldsymbol{v}_1(t,\boldsymbol{r}), \end{aligned}$$

and linearise the single fluid basic equations. Since the medium is unbounded, we perform a Fourier analysis in terms of plane waves and assume that perturbations behave as

$$f_1(\boldsymbol{r},t) = f\mathrm{e}^{\mathrm{i}(\omega t - \boldsymbol{k}\cdot\boldsymbol{r})}. \tag{3}$$

Now, with no loss of generality, we choose the z-axis so that the wavevector $\boldsymbol{k}$ lies in the xz-plane ($\boldsymbol{k} = k_x\hat{\boldsymbol{x}} + k_z\hat{\boldsymbol{z}}$), and introducing the propagation angle, θ, between $\boldsymbol{k}$ and $\boldsymbol{B}_0$, the wavenumber components can be expressed as $k_x = k\cos\theta$ and $k_z = k\sin\theta$. With this approach, the operator $\frac{\partial}{\partial t} + \boldsymbol{v}_0\cdot\nabla$ becomes $\mathrm{i}(\omega - k_x v_0)$, which points out that in the presence of a background flow the frequency has a Doppler shift given by $k_x v_0$ and that the wave frequency, ω, for the case with flow can be obtained from

$$\omega = \Omega + k_x v_0, \tag{4}$$

Ω being the wave frequency in absence of flow. In other words, Ω corresponds to the frequency measured by an observer linked to the flow inertial rest frame, while ω corresponds to the frequency measured by an observer tied to an inertial rest frame external to the flow.

Applying the above stated procedure to the single fluid MHD equations describing a flowing partially ionised plasma in which non-adiabatic processes take place (Forteza et al. 2008; Carbonell et al. 2009), the following scalar equations can be obtained,

$$\Omega\rho_1 - \rho_0(k_x v_{1x} + k_z v_{1z}) = 0, \tag{5}$$

$$\Omega\rho_0 v_{1x} - k_x p_1 = 0, \tag{6}$$

$$\Omega\rho_0 v_{1y} + \frac{B_{0x}}{\mu}k_x B_{1y} = 0, \tag{7}$$

$$\Omega\rho_0 v_{1z} - k_z p_1 + \frac{B_{0x}}{\mu}(k_x B_{1z} - k_z B_{1x}) = 0, \tag{8}$$

$$\begin{aligned}\mathrm{i}\Omega\left(p_1 - c_\mathrm{s}^2\rho_1\right) + (\gamma-1)\left(\kappa_{\mathrm{e}\parallel}k_x^2 + \kappa_\mathrm{n}k^2 + \rho_0 L_\mathrm{T}\right)T_1\\ +(\gamma-1)(L+\rho_0 L_\rho)\rho_1 = 0,\end{aligned} \tag{9}$$

$$\begin{aligned}B_{1x}\left(\mathrm{i}\Omega + k_x^2\eta + k_z^2\eta_\mathrm{C}\right) + (\eta-\eta_\mathrm{C})k_x k_z B_{1z}\\ -B_{0x}k_z(\mathrm{i}v_{1z} - k_z\Xi p_1) = 0,\end{aligned} \tag{10}$$

$$B_{1y}\left(\mathrm{i}\Omega + k_x^2\eta_\mathrm{C} + k_z^2\eta\right) + \mathrm{i}B_{0x}k_x v_{1y} = 0, \tag{11}$$

$$\begin{aligned}B_{1z}\left(\mathrm{i}\Omega + k_x^2\eta_\mathrm{C} + k_z^2\eta\right) + (\eta-\eta_\mathrm{C})k_x k_z B_{1x}\\ +B_{0x}k_x(\mathrm{i}v_{1z} - k_z\Xi p_1) = 0,\end{aligned} \tag{12}$$

$$k_x B_{1x} + k_z B_{1z} = 0, \tag{13}$$

$$\frac{p_1}{p_0} - \frac{\rho_1}{\rho_0} - \frac{T_1}{T_0} = 0. \tag{14}$$

where the quantity Ξ is,

$$\Xi = \frac{\xi_\mathrm{n}^2\xi_\mathrm{i}}{(1+\xi_\mathrm{i})\alpha_n}, \tag{15}$$

with α_n a friction coefficient (Braginskii 1965; Khodachenko et al. 2004; Leake et al. 2005), while the quantity Ξ has been introduced for the reason of compactness of the above linearised equations and its dimensions correspond to the inverse of a friction coefficient. Depending on the value given to $\tilde{\mu}$ and to both Spitzer's (η) and Cowling's (η_C) resistivities, we may have different types of plasmas, and those of interest for our study are:

1. a fully ionised resistive plasma (FIRP), where $\tilde{\mu} = 0.5$, $\eta = \eta_C$ and $\Xi = 0$;
2. a partially ionised plasma (PIP), where $0.5 < \tilde{\mu} < 1$, $\eta \neq \eta_C$ and $\Xi \neq 0$.

Other important parameters of our study are the numerical value and behavior of the sound (c_s) and Alfvén (v_a) speeds. In the case of density and magnetic field assumed in Sect. 2.1, the Alfvén speed has a constant numerical value of 126.15 km s^{-1}. However, since the sound speed depends on gas pressure, which is a function of the number densities of ions and neutrals, its numerical value is not constant but depends on the ionisation fraction considered. For a fully ionised plasma, the sound speed is 14.84 km s^{-1}, while for a partially ionised plasma with $\tilde{\mu} = 0.95$ its value decreases to 10.76 km s^{-1}. This variation in the sound speed can be important since depending on the flow speed and ionisation fraction chosen, the flow speed could be greater than, smaller than, or equal to the sound speed, which affects the direction of propagation of slow and thermal waves (Carbonell et al. 2009). In our case, the flow speed is subalfvénic but slightly supersonic, which seems to be a typical feature of flows observed in quiescent filaments.

3. Alfvén waves

Equations (7) and (11) are decoupled from the rest and from them we can obtain the dispersion relation for Alfvén waves in a partially ionised plasma with a background flow, which is,

$$\Omega^2 - \mathrm{i}\Omega k^2(\eta_C \cos^2\theta + \eta \sin^2\theta) - v_a^2 k^2 \cos^2\theta = 0, \tag{16}$$

where θ is the angle between the wavenumber vector and the magnetic field. In the case of a fully ionised ideal plasma without a background flow, Eq. (16) reduces to the well known dispersion relation for Alfvén waves. Eq. (16) also points out that the time damping of Alfvén waves must be dominated by resistive effects.

Since we are interested in the time damping of MHD waves, we consider the wavenumber, k, to be real and seek for complex solutions of the frequency ω expressed as $\omega = \omega_r + \mathrm{i}\omega_i$. Taking into account Eq. (4) we can conclude that, for an observer external to the flow, the real part of the frequency, ω_r is given by $\omega_r = \Omega_r + k_x v_0$, and that the imaginary part, ω_i, is $\omega_i = \Omega_i$, i.e. the imaginary part of the frequency is the same with or without flow. The period of the waves is given by $P = \frac{2\pi}{\omega_r}$, the damping time by $\tau_D = \frac{1}{\omega_i}$, the ratio of the damping time versus period is $\frac{\tau_D}{P}$, and, in general, unless otherwise is stated, we consider a propagation angle $\theta = \frac{\pi}{8}$. Since in the above calculations we use the real and imaginary parts of the complex frequency, ω, the resultant quantities correspond to the period, damping time and the ratio of the damping time versus period, measured by an observer external to the flow i.e. to what would be determined from the analysis of ground- or space-based observations.

The solution to dispersion relation (16) is,

$$\Omega = \pm\frac{\sqrt{4v_a^2k^2\cos^2\theta - (\eta_C\cos^2\theta + \eta\sin^2\theta)^2k^4}}{2} + \frac{\mathrm{i}k^2(\eta_C\cos^2\theta + \eta\sin^2\theta)}{2}, \tag{17}$$

which written in terms of ω becomes,

$$\omega_{hfb} = k_x v_0 + \frac{\sqrt{4v_a^2k^2\cos^2\theta - (\eta_C\cos^2\theta + \eta\sin^2\theta)^2k^4}}{2} + \frac{\mathrm{i}k^2(\eta_C\cos^2\theta + \eta\sin^2\theta)}{2}, \tag{18}$$

and

$$\omega_{lfb} = k_x v_0 - \frac{\sqrt{4v_a^2k^2\cos^2\theta - (\eta_C\cos^2\theta + \eta\sin^2\theta)^2k^4}}{2} + \frac{\mathrm{i}k^2(\eta_C\cos^2\theta + \eta\sin^2\theta)}{2}, \tag{19}$$

where hfb and lfb mean high frequency and low frequency branch, respectively. In absence of flow ($|\boldsymbol{v}_0| = 0$) there is a critical wavenumber, k_c, at which the real part of the frequency for both branches become zero (apart from the trivial solution). The expression for this critical wavenumber can be obtained from Eq. (17) and is,

$$k_c = \frac{2v_a\cos\theta}{\eta_C\cos^2\theta + \eta\sin^2\theta}. \tag{20}$$

When $k = k_c$ there are no propagating Alfvén waves, only a damped perturbation remains with a purely imaginary frequency given by,

$$\omega_i = \left[\frac{k^2(\eta_C\cos^2\theta + \eta\sin^2\theta)}{2}\right]. \tag{21}$$

When $k > k_c$, there are no propagating Alfvén waves and only two damped perturbation remains whose purely imaginary frequencies are given by,

$$\omega_i = \pm\frac{\sqrt{(\eta_C\cos^2\theta + \eta\sin^2\theta)^2k^4 - 4v_a^2k^2\cos^2\theta}}{2} + \left[\frac{k^2(\eta_C\cos^2\theta + \eta\sin^2\theta)}{2}\right]. \tag{22}$$

However, in presence of flow things become different. The real part of the frequency for the low frequency branch becomes zero for,

$$k_{lfb} = \frac{2\sqrt{v_a^2 - v_0^2}\cos\theta}{\eta_C\cos^2\theta + \eta\sin^2\theta}. \tag{23}$$

Since in our case $c_s < v_0 < v_a$, when $k < k_{lfb}$ the real part of the frequency is negative and the low frequency Alfvén wave propagates towards the negative part of the x-axis; when $k = k_{lfb}$, the low frequency Alfvén wave becomes non propagating, and when $k > k_{lfb}$, the real part of the frequency is positive and the low frequency Alfvén wave propagates towards the positive part of x-axis, with the reversal of the behavior occurring at $k = k_{lfb}$. Furthermore, the square root in Eqs. (18) and (19) becomes zero

when $k = k_c$, with $k_c > k_{lfb}$. For $k = k_c$, both real parts of the high and low frequency branches become $k_x v_0$, while the imaginary parts are given by Eq. (21), however, for $k > k_c$, while the real part of both Alfvén waves is still given by $k_x v_0$, the imaginary parts of the frequency for both branches become,

$$\omega_{i,hfb} = \frac{k^2(\eta_C \cos^2\theta + \eta \sin^2\theta)}{2} + \frac{\sqrt{(\eta_C \cos^2\theta + \eta \sin^2\theta)^2 k^4 - 4v_a^2 k^2 \cos^2\theta}}{2}, \quad (24)$$

and

$$\omega_{i,lfb} = \frac{k^2(\eta_C \cos^2\theta + \eta \sin^2\theta)}{2} - \frac{\sqrt{(\eta_C \cos^2\theta + \eta \sin^2\theta)^2 k^4 - 4v_a^2 k^2 \cos^2\theta}}{2}. \quad (25)$$

Therefore, for $k > k_c$, we end up with two Alfvén waves propagating in the same direction, with the same real frequency ($k_x v_0$) but with different imaginary parts of the frequency i. e. having different damping times.

In the case of a fully ionised ideal plasma with a background flow, the Alfvén frequency is given by,

$$\omega_r = k \cos\theta (v_0 \pm v_a), \quad (26)$$

then, we could try to write the real part of the frequencies (18) and (19) in a similar way. After some algebra, we end up with the following expression,

$$\omega_r = k \cos\theta (v_0 \pm V_a), \quad (27)$$

with

$$V_a = v_a \times \sqrt{1 - \frac{(\eta_C \cos^2\theta + \eta \sin^2\theta)^2 k^2}{4v_a^2 \cos^2\theta}}. \quad (28)$$

Since the square root is non-dimensional, V_a can be understood as a modified Alfvén speed, and once the physical conditions have been fixed, this modified Alfvén speed only depends on the wavenumber k. From Eq. (27), the real frequencies for both waves can be written as,

$$\omega_{hfb} = k \cos\theta (v_0 + V_a), \quad (29)$$

and

$$\omega_{lfb} = k \cos\theta (v_0 - V_a). \quad (30)$$

Therefore, the periods, $P_\pm$, of both Alfvén waves would be given by,

$$P_\pm = \frac{2\pi}{k \cos\theta (v_0 \pm V_a)}. \quad (31)$$

Using Eqs. (29) and (30), we can understand in a different way when the critical wavenumbers, k_{lfb} and k_c, found above, appear. The critical wavenumber k_{lfb} is a solution of $v_0 - V_a = 0$, while the other critical wavenumber k_c comes from $V_a = 0$. When $k > k_c$, the modified Alfvén speed, V_a, becomes imaginary, and the real part of the frequency for both Alfvén waves becomes $k_x v_0$. Of course, the wavenumbers k_c and k_{lfb} obtained by solving the above equations are exactly the same as in Eqs. (20) and (23).

The above described behavior can be also seen, for instance, in the magnetic field perturbation B_{1y}. Using, Eqs. (3), (18) and (19), the general expression for this perturbation would be,

$$B_{1y} = \tilde{b}_{1y} \exp\left(-\frac{k^2(\eta_C \cos^2\theta + \eta \sin^2\theta)}{2} t\right) \times \exp \mathrm{i}\left(\omega_\pm t - \boldsymbol{k}\cdot\boldsymbol{r}\right), \quad (32)$$

which corresponds to two damped propagating waves with two different real frequency $\omega_\pm$ given by,

$$\omega_\pm = k_x v_0 \pm \frac{\sqrt{4v_a^2 k^2 \cos^2\theta - (\eta_C \cos^2\theta + \eta \sin^2\theta)^2 k^4}}{2}, \quad (33)$$

but with a complex amplitude $\tilde{b}_{1y}$, which can be obtained from Eqs. (7) and (11) once the frequency has been substituted, which decays in time at the same rate for both waves. When $k = k_c$, we have,

$$B_{1y} = \tilde{b}_{1y} \exp\left(-\frac{k^2(\eta_C \cos^2\theta + \eta \sin^2\theta)}{2} t\right) \times \exp \mathrm{i}(k_x v_0 t - \boldsymbol{k}\cdot\boldsymbol{r}), \quad (34)$$

representing two damped waves propagating with a phase speed v_0, and having the same damping time. When $k > k_c$, the perturbations of the magnetic field are given by,

$$B_{1y} = \tilde{b}_{1y} \exp\left(-\frac{k^2(\eta_C \cos^2\theta + \eta \sin^2\theta)}{2} t\right) \times \exp\left(\pm\frac{\sqrt{4v_a^2 k^2 \cos^2\theta - (\eta_C \cos^2\theta + \eta \sin^2\theta)^2 k^4}}{2} t\right) \times \exp \mathrm{i}(k_x v_0 t - \boldsymbol{k}\cdot\boldsymbol{r}), \quad (35)$$

representing two propagating waves with the same real frequency but different damping times. Finally, when $k = k_{lfb}$, we obtain

$$B_{1y} = \tilde{b}_{1y} \exp\left(-\frac{k^2(\eta_C \cos^2\theta + \eta \sin^2\theta)}{2} t\right) \times \exp(-\mathrm{i}\boldsymbol{k}\cdot\boldsymbol{r}), \quad (36)$$

which could also be written as,

$$B_{1y} = \tilde{b}_{1y} \exp\left(-\frac{k^2(\eta_C \cos^2\theta + \eta \sin^2\theta)}{2} t\right) \cos(\boldsymbol{k}\cdot\boldsymbol{r}), \quad (37)$$

representing a damped disturbance, but not a propagating wave.

Summarizing, without flow Alfvén waves become non propagating for $k \geq k_c$. For $k = k_c$ only a damped perturbation remains, while for $k > k_c$ two damped perturbations, with different damping times, remain. On the contrary, the presence of flow allows both Alfvén waves to be always propagating waves for an external observer, and for wavenumbers greater than k_c both have the same real frequency ($k_x v_0$), but two different imaginary parts, and we can conclude that the joint action of flow and partial ionisation strongly modifies the behavior of Alfvén waves. Furthermore, it is worth to remark that in absence of flow, $k_{lfb} = k_c$ (see Eqs. (20) and (23)), and both Alfvén branches behave in the same way.

Figure 1 displays the period, damping time and the ratio of damping time to period versus the wavenumber and confirms the above analytical results. This figure shows the unfolding

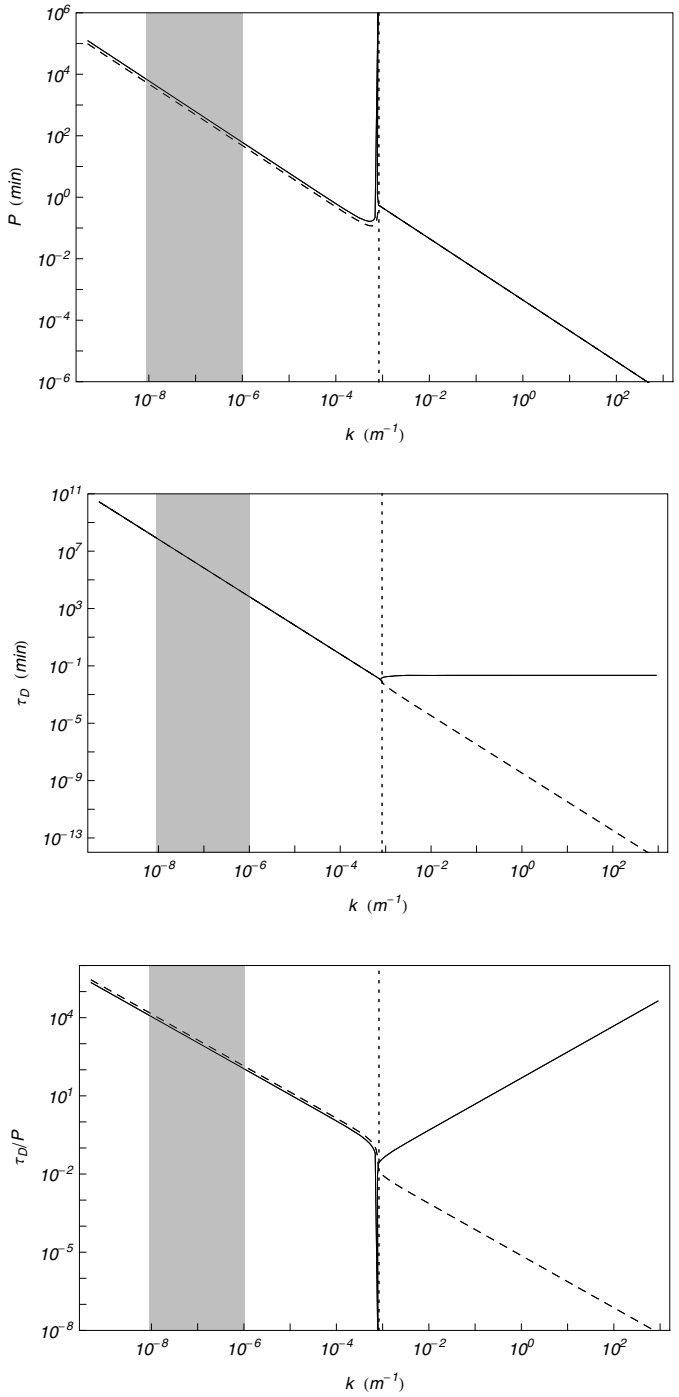

Fig. 1. Period, damping time, and ratio of the damping time to period versus the wavenumber for the long (solid) and short (dashed) period Alfvén waves in a PIP with $\tilde{\mu} = 0.8$. In all the panels, the location of the critical wavenumber, k_c, is defined by the vertical dotted line. The background flow speed is 15 km s^{-1} and the shaded region corresponds to the interval of observed wavelengths in prominence oscillations.

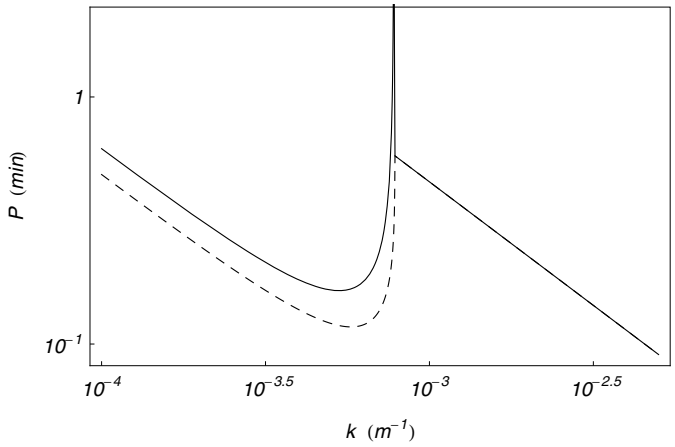

Fig. 2. Period versus wavenumber for Alfvén waves in a PIP with $\tilde{\mu} = 0.8$: zoom of the region around the critical wavenumbers $k_{\rm lfb}$ and k_c, showing the behavior of the periods for the high-(solid) and low-(dashed) period branches. For $k > k_c$ both branches (solid) have the same period. The background flow speed is 15 km s^{-1}.

in period due to the flow and the behavior of the period, for both waves, around the critical wavenumbers. For wavenumbers larger than k_c, both waves display the same period. Also, in the case of the damping time it can be seen that once the critical wavenumber k_c is attained we are left with two different damping times for wavenumbers larger than k_c. One damping time is almost constant while the other decreases in a continuous way. Of course, the ratio τ_D/P has also two branches which behave quite differently for wavenumbers larger than k_c. Furthermore, we can also observe that the critical wavenumbers, $k_{\rm lfb}$ and k_c, are outside the region of observed wavelengths in prominence oscillations. Regarding the damping time of Alfvén waves, Figure 1 clearly shows that, within the range of observed wavelengths, it is very large and quite incompatible with the up to now reported damping times from observations. The same happens with the ratio between the damping time and the period. This clearly points out that, at least within the range of observed wavelengths in prominence oscillations, the ion-neutral collisions mechanism can not provide with an explanation for the time damping of Alfvén waves in partially ionised prominence plasmas. It is also of interest to point out that in most of the figures, the location of the critical wavenumbers is defined by the presence of peaks and bifurcations in the different plots. Figure 2 shows in a more clear way the behavior of the period for both waves in a region located around the two critical wavenumbers $k_{\rm lfb}$ and k_c.

On the other hand, Fig. 3 displays the behaviors of the modified Alfvén speed, V_a, and the period of the low-period branch of Alfvén waves, computed from Eq. (31), versus the wavenumber k. The modified Alfvén speed is almost constant, close to the value of the Alfvén speed, v_a, for a large range of wavenumbers. However, for wavenumbers larger than 10^{-4} m^{-1} it starts to decrease rapidly going to zero at $k = k_c$. It is interesting to remark that since the Alfvén speed v_a is determined by some of the characteristic quantities of the plasma (magnetic field and density), once these parameters have been fixed v_a remains constant. However, the modified Alfvén speed, V_a, depends on the wavenumber and, for a fixed wavenumber and propagation angle, the Alfvén wave would propagate with the modified Alfvén speed. Regarding the period, we can observe an excellent agreement with the behavior of the exact period shown in Fig. 1 and at $k = k_c$, when the modified Alfvén speed vanishes, it would jump to a period given by $2\pi/k_x v_0$.

The existence of a critical wavenumber in fully ionised resistive plasmas was already pointed out by Ferraro & Plumpton (1961), Chandrasekhar (1961), Kendall & Plumpton (1964), while for partially ionised plasmas it was already reported by Balsara (1996), in the context of waves in molecular clouds, and by Forteza et al. (2008), Singh & Krishnan (2009) and Soler et al. (2009c,d,e) in the case of MHD waves in solar coronal structures.

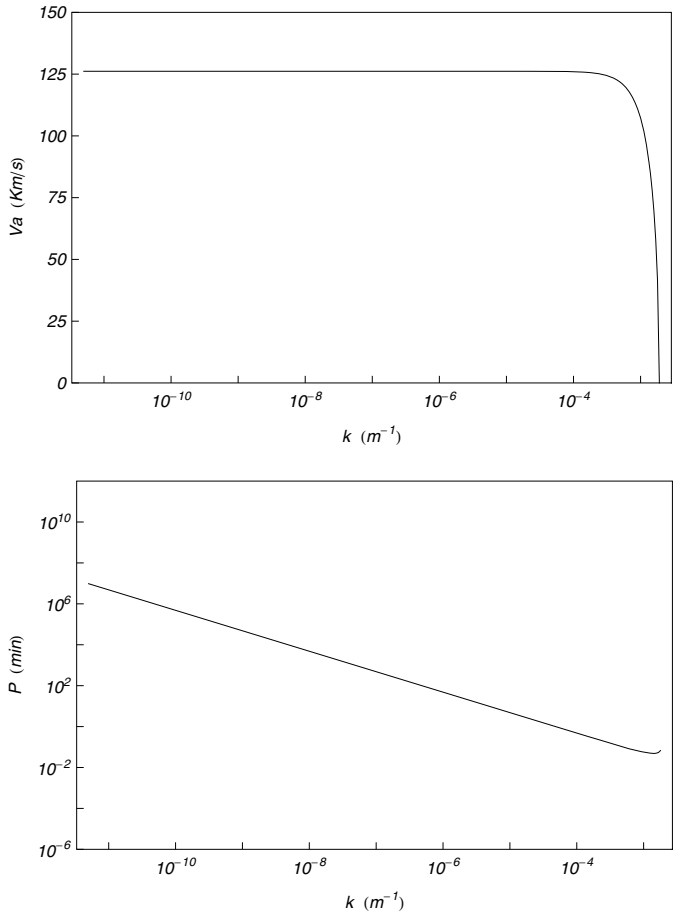

Fig. 3. Modified Alfvén speed and period of the low-period Alfvén wave versus wavenumber, obtained from Eqs. (28) and (31).

The behavior of finite critical wavenumber in a partially ionised plasma can be understood by writing its expression in terms of η and η_C. The Cowling magnetic diffusivity, η_C, is,

$$\eta_C = \frac{1}{\mu_0}\left[\frac{m_e}{n_e e^2}\left(\frac{1}{\tau_{ei}}+\frac{1}{\tau_{en}}\right)+\frac{\xi_n^2 B_0^2}{\alpha_n}\right], \tag{38}$$

where τ_{en} and τ_{ei} are the electron-neutral and electron-ion collisional times, respectively. On the other hand, α_n is a friction coefficient whose expression is,

$$\alpha_n = \frac{1}{2}\xi_n(1-\xi_n)\frac{\rho_0^2}{m_n}\sqrt{\frac{16 k_B T_0}{\pi m_i}}\Sigma_{in}, \tag{39}$$

with Σ_{in} the ion-neutral cross-section. The Spitzer magnetic diffusivity, η, is,

$$\eta = \frac{1}{\mu_0}\left[\frac{m_e}{n_e e^2}\left(\frac{1}{\tau_{ei}}+\frac{1}{\tau_{en}}\right)\right], \tag{40}$$

then, the critical wavenumber, k_c, given by Eq. (20), becomes,

$$k_c = \frac{2 v_a \cos\theta}{\frac{1}{\mu_0}\left[\frac{m_e}{n_e e^2}\left(\frac{1}{\tau_{ei}}+\frac{1}{\tau_{en}}\right)+\frac{\xi_n^2 B_0^2}{\alpha_n}\cos^2\theta\right]}. \tag{41}$$

In the case of a fully ionised resistive plasma, the collisional time between electrons and neutrals becomes infinite and the terms corresponding to partial ionisation disappear, so, the critical wavenumber is only determined by the electron-ion collisional time. Taking into account that $\eta_C \gg \eta$, the critical wavenumber in the case of a partially ionised plasma is smaller than in the case of a fully ionised resistive plasma. Finally, it is worth to remark than when a fully ionised ideal plasma is considered, no critical wavenumber appears due to the fact that the magnetic diffusivity is considered negligible, however, since the ion-electron collisional time depends on temperature, only for very large values of the temperature the ion-electron collisional time would be very large making magnetic diffusivity negligible, i.e. there is always a critical wavenumber since the electron-ion collisional time, τ_{ei}, never attains an infinite value.

On the other hand, both critical wavenumbers, k_{lfb} and k_c, could be also written in terms of the magnetic Reynolds number. In a partially ionised plasma, Cowling's magnetic diffusivity, η_C, is several orders of magnitude greater than Spitzer's magnetic diffusivity, η, therefore, neglecting η in the expression under the square root in Eqs. (18) and (19), and computing again the expresion for the wavenumber k_c, we obtain,

$$k_c = \frac{2 v_a}{\eta_C \cos\theta}. \tag{42}$$

In our case, the magnetic Reynolds number, R_m, could be written as $R_m = uL/\eta_C$, where u is a characteristic velocity, which we could take as the Alfvén speed, and L is a characteristic scale-length. Then, R_m can be expressed as $R_m = v_a L/\eta_C$, and using Eq. (42) we obtain,

$$k_c = \frac{2R_m}{L\cos\theta}. \tag{43}$$

Following the same approach, the wavenumber k_{lfb} can be written as,

$$k_{lfb} = \frac{2R_m}{L\cos\theta}\sqrt{1-\left(\frac{v_0}{v_a}\right)^2}. \tag{44}$$

Then, when flow is absent $k_c = k_{lfb}$, and, furthermore, these expressions point out, again, that for a fully ionised ideal plasma, both critical wavenumbers become very large because of the magnetic Reynolds number.

Finally, if we consider a FIRP all the computed expressions for Alfvén waves need to be modified by taking into account that in this case $\eta_C = \eta$. Then, only Spitzer's magnetic diffusivity will be responsible for the damping of Alfvén waves and, since this resistivity is much smaller than Cowling's resistivity in a PIP, we can expect that the critical wavenumbers are going to be displaced towards the region of large wavenumbers. This is exactly what is shown in Fig. 4. Furthermore, in this figure we can also observe that the periods of the Alfvén waves in a FIRP are similar to those in a PIP, while the damping time is much greater because of the smaller value of Spitzer's resistivity compared with Cowling's resistivity.

4. Magnetoacoustic waves

From the rest of linearised equations, and assumig that the determinant of the algebraic system is zero, we obtain our general dispersion relation for thermal and magnetoacoustic waves in presence of a background flow, which is given by,

$$(\Omega^2 - k^2\Lambda^2)(\mathrm{i}k^2\eta_C\Omega - \Omega^2) + k^2 v_a^2(\Omega^2 - k_x^2\Lambda^2) + \mathrm{i}k^2 k_z^2 v_a^2\Lambda^2\Xi\rho_0\Omega = 0, \tag{45}$$

where Λ^2 is the non-adiabatic sound speed squared (Forteza et al. 2008; Soler et al. 2008; Soler 2010) defined as

$$\Lambda^2 = \frac{c_s^2}{\gamma}\left[\frac{(\gamma-1)(\bar{\kappa}_{e\|}k_x^2 + \bar{\kappa}_n k^2 + \omega_T - \omega_\rho) + \mathrm{i}\gamma\Omega}{(\gamma-1)(\bar{\kappa}_{e\|}k_x^2 + \bar{\kappa}_n k^2 + \omega_T) + \mathrm{i}\Omega}\right], \tag{46}$$

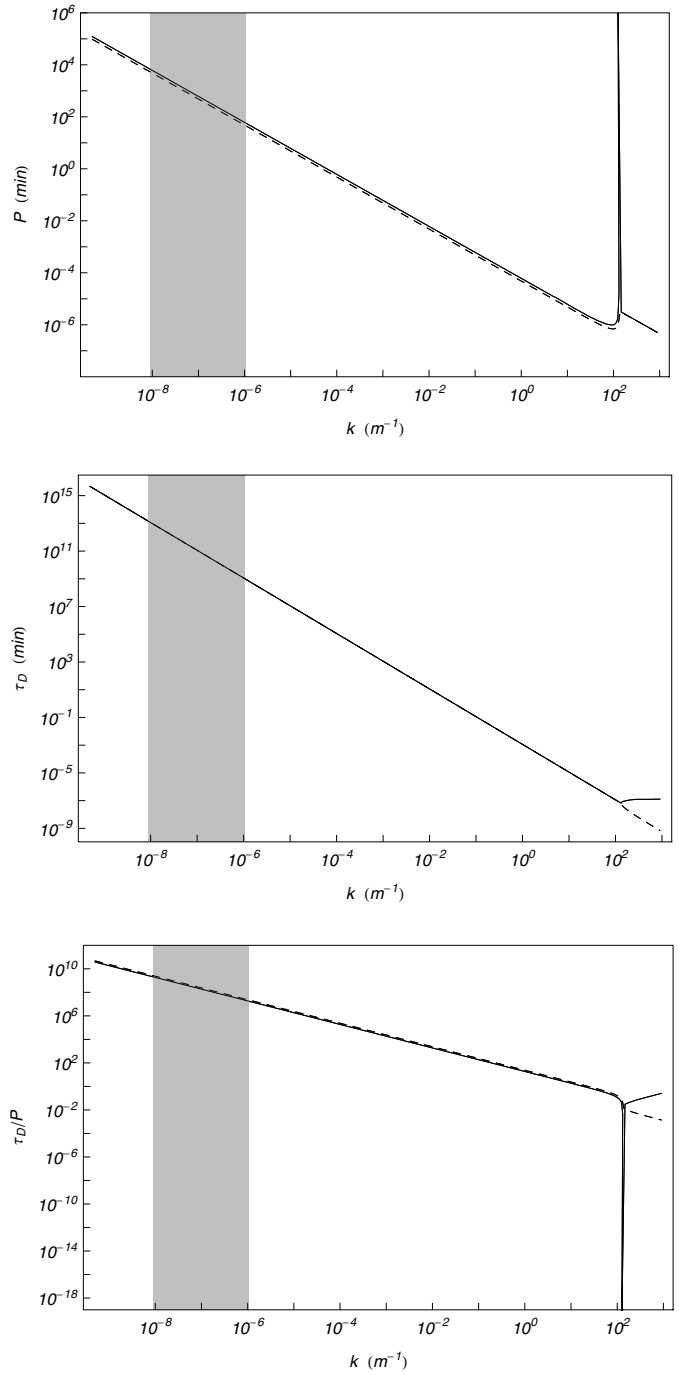

Fig. 4. Period, damping time, and ratio of the damping time to period versus the wavenumber for the long (solid) and short (dashed) period Alfvén waves in a FIRP ($\tilde{\mu} = 0.5$). The location of the critical wavenumbers is defined by the presence of peaks and bifurcations in the plots. The background flow speed is 15 km s^{-1} and the shaded region corresponds to the interval of observed wavelengths in prominence oscillations.

with

$$\bar{\kappa}_{e\|} = \frac{T_0}{p_0}\kappa_{e\|}, \quad \bar{\kappa}_n = \frac{T_0}{p_0}\kappa_n$$
$$\omega_\rho = \frac{\rho_0}{p_0}\rho_0 L_\rho, \quad \omega_T = \frac{\rho_0}{p_0}T_0 L_T$$

and where the effects of optically thin radiative losses, thermal conduction by electrons and neutrals, and a constant heating per unit volume are included. When Eq. (45) is expanded, it becomes a fifth degree polynomial in the frequency Ω. By setting the appropriate values to the corresponding quantities, the dispersion relation (45) is consistent with the case of an adiabatic and partially ionised plasma without flow (Forteza et al. 2007), the case of a non-adiabatic and partially ionised plasma without flow (Forteza et al. 2008) and the case of a non-adiabatic, fully ionised plasma with a background flow (Carbonell et al. 2009). In the following, we are going to solve the above dispersion for two different cases: Fully ionised resistive plasma (FIRP) and partially ionised plasma (PIP).

4.1. Fully ionised resistive plasma

In this case, the dispersion relation becomes

$$(\Omega^2 - k^2\Lambda^2)(ik^2\eta\Omega - \Omega^2) + k^2 v_a^2(\Omega^2 - k_x^2\Lambda^2) = 0, \tag{47}$$

which is a fifth degree polynomial in the frequency Ω. Considering only longitudinal propagation ($\theta = 0$), the above dispersion relation becomes,

$$(\Omega^2 - k_x^2\Lambda^2)(ik^2\eta\Omega - \Omega^2 + k^2 v_a^2) = 0, \tag{48}$$

By setting the expression within the first bracket equal to zero we obtain,

$$\Omega^2 - k_x^2\Lambda^2 = 0, \tag{49}$$

which is the dispersion relation corresponding to coupled slow and thermal waves, modified by the flow and damped by thermal effects, and which points out that when perpendicular propagation is not allowed magnetic diffusivity does not influence the behavior of slow or thermal waves. Setting now the expression within the second bracket equal to zero, we obtain the dispersion relation (16), with $\theta = 0$ and $\eta = \eta_C$, corresponding to the Alfvén waves already studied in Sect. 3.

Figure 5 displays the period, damping time and the ratio of damping time to period versus the wavenumber for magnetoacoustic and thermal waves for a FIRP with parallel propagation. Because of parallel propagation and since only Spitzer's resistivity is present, fast waves in Fig. 5 behave exactly in the same way as Alfvén waves in Fig. 4. On the other hand, we can clearly observe the unfolding of the period for slow waves and the distorsion appearing in the behavior of the period corresponding to the high-period slow wave which was already explained in Carbonell et al. (2009). In the case of the damping time, slow and thermal waves are damped only by non-adiabatic effects, while the damping of fast waves is governed by resistive effects since they behave like pure Alfvén waves.

In order to obtain an analytical expression for the imaginary part of the slow mode frequency, we must keep in mind that the presence of flow only modifies the real part of the frequency. For this reason, we can take the dispersion relation given by Eq. (49) which when flow is absent becomes,

$$\omega^2 - k_x^2\Lambda^2 = 0, \tag{50}$$

then, considering that $\omega = \omega_r + i\omega_i$ and assuming that the damping is weak ($\omega_i \ll \omega_r$) we neglect terms in ω_i^2 and ω_i^3. Following this approach, we obtain,

$$\omega_i = \frac{\gamma - 1}{2\gamma}\left[\frac{(\gamma-1)(\bar{\kappa}_{e\|}k_x^2 + \omega_T) + \omega_\rho}{(\gamma-1)^2(\bar{\kappa}_{e\|}k_x^2 + \omega_T)^2 + c_s^2 k_x^2}\right]c_s^2 k_x^2, \tag{51}$$

which is equal to the imaginary part of the frequency when a flow is present.

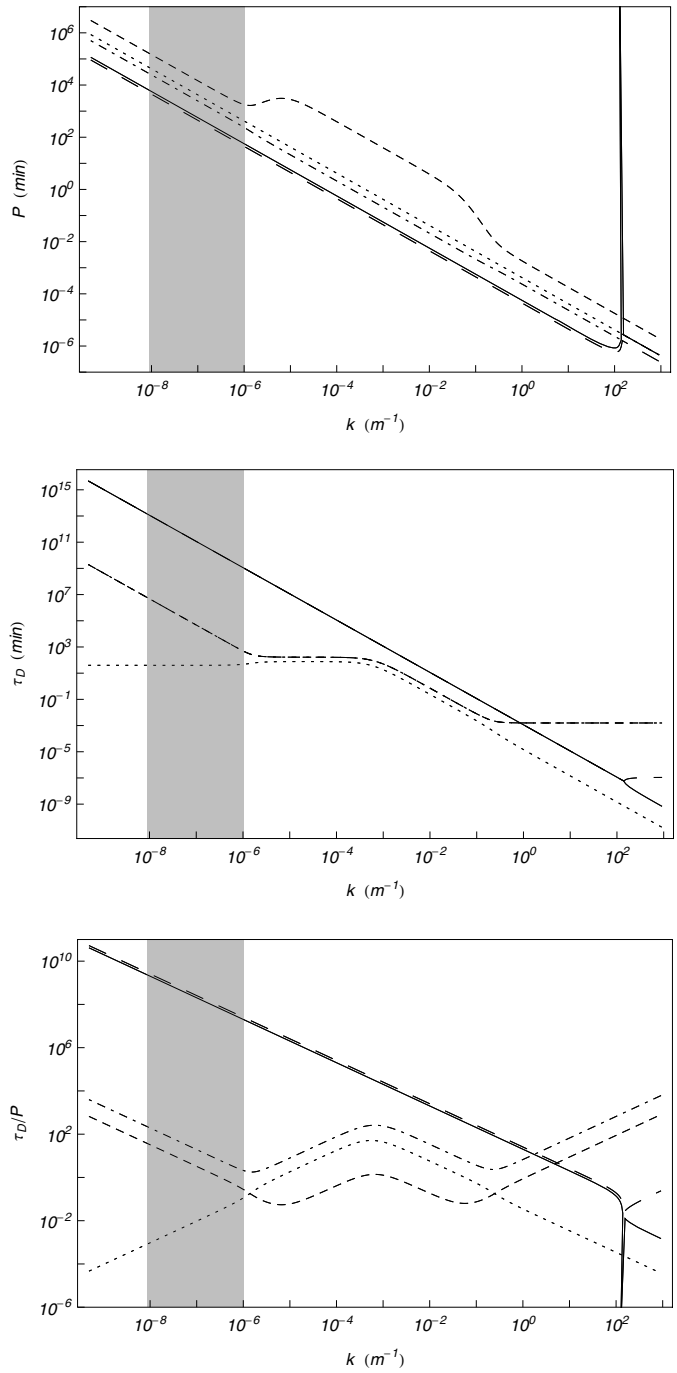

Fig. 5. Period, damping time, and ratio of the damping time to period versus the wavenumber for magnetoacoustic waves in a FIRP ($\tilde{\mu} = 0.5$) and $\theta = 0$. Slow waves (short-dashed and dot-dashed lines), fast waves (continuous and long-dashed lines), thermal wave (dotted line). The location of the critical wavenumbers is defined by the presence of peaks and bifurcations in the plots. The background flow speed is 15 km s^{-1} and the shaded region corresponds to the interval of observed wavelengths in prominence oscillations.

Now, following a similar approach we could calculate analytical approximations to the imaginary part of the thermal wave frequency, and to this end, we expand Eq. (50) obtaining,

$$\omega^3 - \mathrm{i}(\gamma-1)(\bar{\kappa}_{\mathrm{e}\parallel}k_x^2 + \omega_{\mathrm{T}})\omega^2 - k_x^2 c_{\mathrm{s}}^2 \omega + \mathrm{i}k_x^2\left[\frac{p_0(\gamma-1)\left(\bar{\kappa}_{\mathrm{e}\parallel}k_x^2 + \omega_{\mathrm{T}} - \omega_\rho\right)}{\rho_0}\right] = 0. \tag{52}$$

For small parallel wavenumbers, the above expression gives,

$$\omega_{\mathrm{i}} = (\gamma-1)\omega_{\mathrm{T}}, \tag{53}$$

while for large parallel wavenumbers it becomes,

$$\omega_{\mathrm{i}} = \frac{\gamma-1}{\gamma}\left[\bar{\kappa}_{\mathrm{e}\parallel}k_x^2 + \omega_{\mathrm{T}} - \omega_\rho\right]. \tag{54}$$

Using Eq. (46), we could compute the limit values of the non-adiabatic sound speed for small and large k_x, obtaining

$$\Lambda^2 = \frac{c_{\mathrm{s}}^2}{\gamma}\frac{\omega_{\mathrm{T}} - \omega_\rho}{\omega_{\mathrm{T}}} = \frac{p_0}{\rho_0}\frac{\omega_{\mathrm{T}} - \omega_\rho}{\omega_{\mathrm{T}}}, \tag{55}$$

for small k_x and

$$\Lambda^2 = \frac{c_{\mathrm{s}}^2}{\gamma} = \frac{p_0}{\rho_0}, \tag{56}$$

for large k_x, corresponding to the isothermal sound speed. Now, taking into account the flow, we could try to compute analytical approximations for the ratio of the damping time versus period (τ_{D}/P) for slow and thermal waves. For small k_x, the real part of the slow wave frequency is given by,

$$\omega_{\mathrm{r}} \sim k_x\left(v_0 \pm \sqrt{\frac{\omega_{\mathrm{T}} - \omega_\rho}{\gamma\omega_{\mathrm{T}}}}c_{\mathrm{s}}\right), \tag{57}$$

and using Eq. (51) we can obtain

$$\frac{\tau_{\mathrm{D}}}{P} \sim \frac{\gamma}{\pi}\left[\frac{(\gamma-1)\frac{\omega_{\mathrm{T}}^2}{\omega_\rho}}{(\gamma-1)\frac{\omega_{\mathrm{T}}}{\omega_\rho}+1}\right]\frac{v_0 \pm \sqrt{\frac{\omega_{\mathrm{T}}-\omega_\rho}{\gamma\omega_{\mathrm{T}}}}c_{\mathrm{s}}}{c_{\mathrm{s}}^2}k_x^{-1}, \tag{58}$$

while for large k_x,

$$\omega_{\mathrm{r}} \sim k_x\left(v_0 \pm \frac{c_{\mathrm{s}}}{\sqrt{\gamma}}\right), \tag{59}$$

and, we obtain

$$\frac{\tau_{\mathrm{D}}}{P} \sim \frac{\gamma}{\pi}\bar{\kappa}_{\mathrm{e}\parallel}\frac{v_0 \pm \frac{1}{\sqrt{\gamma}}c_{\mathrm{s}}}{c_{\mathrm{s}}^2}k_x. \tag{60}$$

In Eq. (58), the ratio τ_{D}/P is inversely proportional to the wavenumber k_x, while in Eq. (60) the ratio is proportional to the wavenumber k_x. These behaviours can be checked in Fig. 5 in which, for small and large wavenumbers, the ratio τ_{D}/P for slow waves increases in a linear way with k. For the thermal wave, the real part of the frequency is given by,

$$\omega_{\mathrm{r}} = k_x v_0, \tag{61}$$

since in presence of flow it becomes a propagating wave (Carbonell et al. 2009). Then, using Eqs. (53) and (54), we could also compute the approximate expressions for τ_{D}/P, obtaining

$$\frac{\tau_{\mathrm{D}}}{P} \sim \frac{k_x v_0}{2\pi(\gamma-1)\omega_{\mathrm{T}}}, \tag{62}$$

for small k_x, and

$$\frac{\tau_{\mathrm{D}}}{P} \sim \frac{\gamma k_x v_0}{2\pi(\gamma-1)(\bar{\kappa}_{\mathrm{e}\parallel}k_x^2 + \omega_{\mathrm{T}} - \omega_\rho)}, \tag{63}$$

for large k_x. In Eq. (62), the ratio τ_{D}/P is now proportional to the wavenumber k_x, while in Eq. (63) it is inversely proportional

to k_x. Therefore, for large and small wavenumbers the ratio τ_D/P for the thermal wave decreases such as can be seen in Fig. 5.

Finally, for any value of the propagation angle, fast, slow and thermal waves are coupled and the frequencies must be obtained by solving the dispersion relation given by Eq. (47) which once expanded becomes,

$$\Omega^5 - \frac{\mathrm{i}(AT_0 + k^2 p_0 \eta)}{p_0}\Omega^4 - \frac{k^2\left[p_0(c_s^2 + v_a^2) + AT_0\eta\right]}{p_0}\Omega^3 + \frac{1}{p_0\rho_0}\mathrm{i}k^2\left[AT_0(p_0 + v_a^2\rho_0) + p_0\rho_0(c_s^2k^2\eta - H)\right]\Omega^2 + \frac{1}{\rho_0}k^2\left[\rho_0\left(c_s^2k_x^2v_a^2 - Hk^2\eta\right) + AT_0k^2\eta\right]\Omega + \frac{\mathrm{i}k_x^2k^2v_a^2(H\rho_0 - AT_0)}{\rho_0} = 0, \quad (64)$$

where,

$$AT_0 = (\gamma - 1)(\bar{\kappa}_{e\|}k_x^2 + \omega_T)p_0, \quad (65)$$

$$H\rho_0 = (\gamma - 1)p_0\omega_\rho. \quad (66)$$

Figure 6 displays the period, damping time and the ratio of damping time to period versus the wavenumber for magnetoacoustic and thermal waves obtained from Eq. (64). Now, all the waves are coupled and this fact is reflected in the behavior of the damping times for fast and slow waves. At small wavenumbers, the damping time of fast waves is affected by thermal effects and additional distortions, with respect to the uncoupled case, appear for slow waves at large wavenumbers. On the contrary, the thermal wave is not affected by the coupling. Regarding the damping ratio, Fig. 6 shows that, within the region of interest, it is very large for fast waves, very small for the thermal wave, but for wavenumbers between 10^{-7} and 10^{-6} m^{-1} slow waves have a damping ratio close to those found in observations. However, this ratio correspond to very long period oscillations having a more or less similar damping time.

In this case, and following the same approach as before, we could also obtain an approximate expression for the imaginary part of the frequency corresponding to the thermal wave. For small wavenumbers, it is given again by Eq. (53), while for large wavenumbers it becomes,

$$\omega_i = \frac{v_a^2\cos^2\theta(AT_0 - H\rho_0)}{c_s^2v_a^2\rho_0\cos^2\theta + (AT_0 - H\rho_0)\eta}, \quad (67)$$

which shows that Spitzer's magnetic diffusivity influences the behavior of the damping time of the thermal wave in the case of large wavenumbers. Now, following previous approach we can write the approximate expressions for the ratio between the damping time and the period, which are given by Eq. (62) for small wavenumbers, and

$$\frac{\tau_D}{P} \sim \frac{k_x v_0\left[c_s^2v_a^2\rho_0\cos^2\theta + (AT_0 - H\rho_0)\eta\right]}{2\pi v_a^2\cos^2\theta(AT_0 - H\rho_0)}, \quad (68)$$

for large wavenumbers. Such as before, Eq. (62) points out that the ratio τ_D/P is proportional to the wavenumber k_x, while from Eq. (68) we can find that the ratio is again inversely proportional to k_x. These analytical results are coincident with the behaviour, for small and large wavenumbers, of the ratio τ_D/P for the thermal wave shown in Fig. 6.

4.2. Partially ionised plasma

The dispersion relation is now given by Eq. (45) which once expanded becomes,

$$\Omega^5 - \frac{\mathrm{i}(AT_0 + k^2p_0\eta_C)}{p_0}\Omega^4 - \frac{k^2\left[p_0(c_s^2 + v_a^2) + AT_0\eta_C\right]}{p_0}\Omega^3 + \frac{1}{p_0\rho_0}\mathrm{i}k^2\left[AT_0(p_0 + v_a^2\rho_0) + p_0\rho_0\left(c_s^2k^2\eta_C - H - c_s^2v_a^2k_z^2\Xi\rho_0\right)\right]\Omega^2 + \frac{1}{\rho_0}k^2\left[\rho_0\left(c_s^2k_x^2v_a^2 - Hk^2\eta_C + Hk_z^2v_a^2\Xi\rho_0\right) + AT_0\left(k_x^2\eta_C + k_z^2(\eta_C - v_a^2\Xi\rho_0)\right)\right]\Omega + \frac{\mathrm{i}k_x^2k^2v_a^2(H\rho_0 - AT_0)}{\rho_0} = 0, \quad (69)$$

describing coupled slow, thermal and fast waves, with

$$AT_0 = (\gamma - 1)(\bar{\kappa}_{e\|}k_x^2 + \bar{\kappa}_n k^2 + \omega_T)p_0, \quad (70)$$

$$H\rho_0 = (\gamma - 1)p_0\omega_\rho, \quad (71)$$

where thermal conduction and radiative losses produced by neutrals have been included.

For parallel propagation, slow and thermal waves are described by Eq. (49) while fast waves, in this case Alfvén waves, are described by Eq. (16), with $\theta = 0$, and its solutions have been already studied in Sect. 3. In order to calculate approximate expressions for the imaginary part of the frequency for slow waves, we can follow the procedure of Sect. 4.1 obtaining,

$$\omega_i = \frac{\gamma - 1}{2\gamma} \times \left[\frac{(\gamma - 1)(\bar{\kappa}_{e\|}k_x^2 + \bar{\kappa}_n k^2 + \omega_T) + \omega_\rho}{(\gamma - 1)^2(\bar{\kappa}_{e\|}k_x^2 + \bar{\kappa}_n k^2 + \omega_T)^2 + c_s^2k_x^2}\right]c_s^2k_x^2, \quad (72)$$

while the real part of the frequency, for small and large k_x, is given by $\omega_r = k_x(v_0 \pm \Lambda_r)$ with Λ_r, the real part of the non-adiabatic sound speed Λ given by Eqs. (55) and (56). Then, using Eqs. (57), (59) and (72), we can calculate, for small and large wavenumbers, the ratio τ_D/P for slow waves. In the limit of small wavenumbers, the ratio is proportional to k_x^{-1}, while for large wavenumbers it is proportional to k_x. For the thermal wave, the approximate expressions for the imaginary part of the frequency are given by Eqs. (53), for small wavenumbers, and,

$$\omega_i = \frac{v_a^2(AT_0 - H\rho_0)}{\rho_0c_s^2v_a^2 + (AT_0 - H\rho_0)\eta_C}, \quad (73)$$

for large wavenumbers, which shows that Cowling's magnetic diffusivity influences the damping time of the thermal wave for large wavenumbers, and the behavior of the ratio τ_D/P is similar to the case of a FIRP.

Next, and for non-parallel propagation, we can solve numerically the dispersion relation (69) and obtain the periods, damping times and the ratio of damping time to period for each wave. Figure 7 displays the period, damping time and the ratio of damping time to period versus the wavenumber for magnetoacoustic and thermal waves. We can observe that the results are

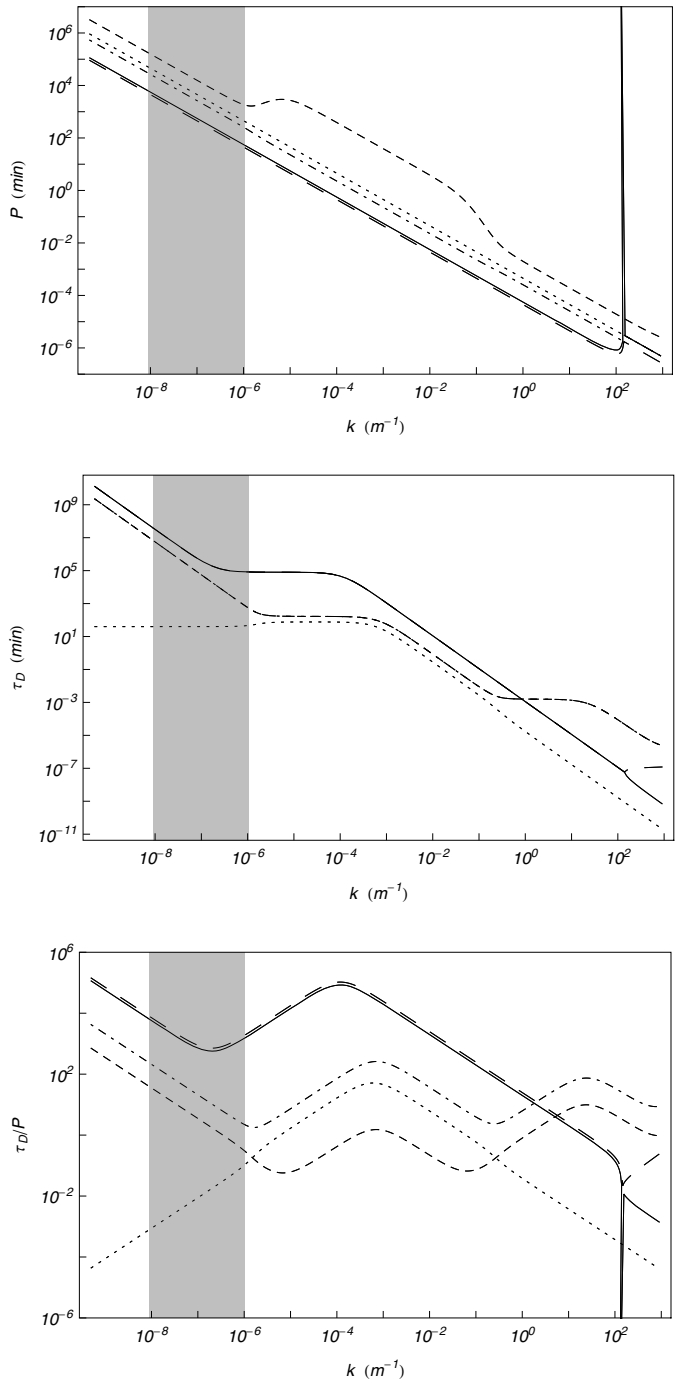

Fig. 6. Period, damping time, and ratio of the damping time to period versus the wavenumber for magnetoacoustic waves in a FIRP ($\tilde{\mu} = 0.5$). Slow waves (short-dashed and dot-dashed lines), fast waves (continuous and long-dashed lines), thermal wave (dotted line). The location of the critical wavenumbers is defined by the presence of peaks and bifurcations in the plots. The background flow speed is 15 km s^{-1} and the shaded region corresponds to the interval of observed wavelengths in prominence oscillations.

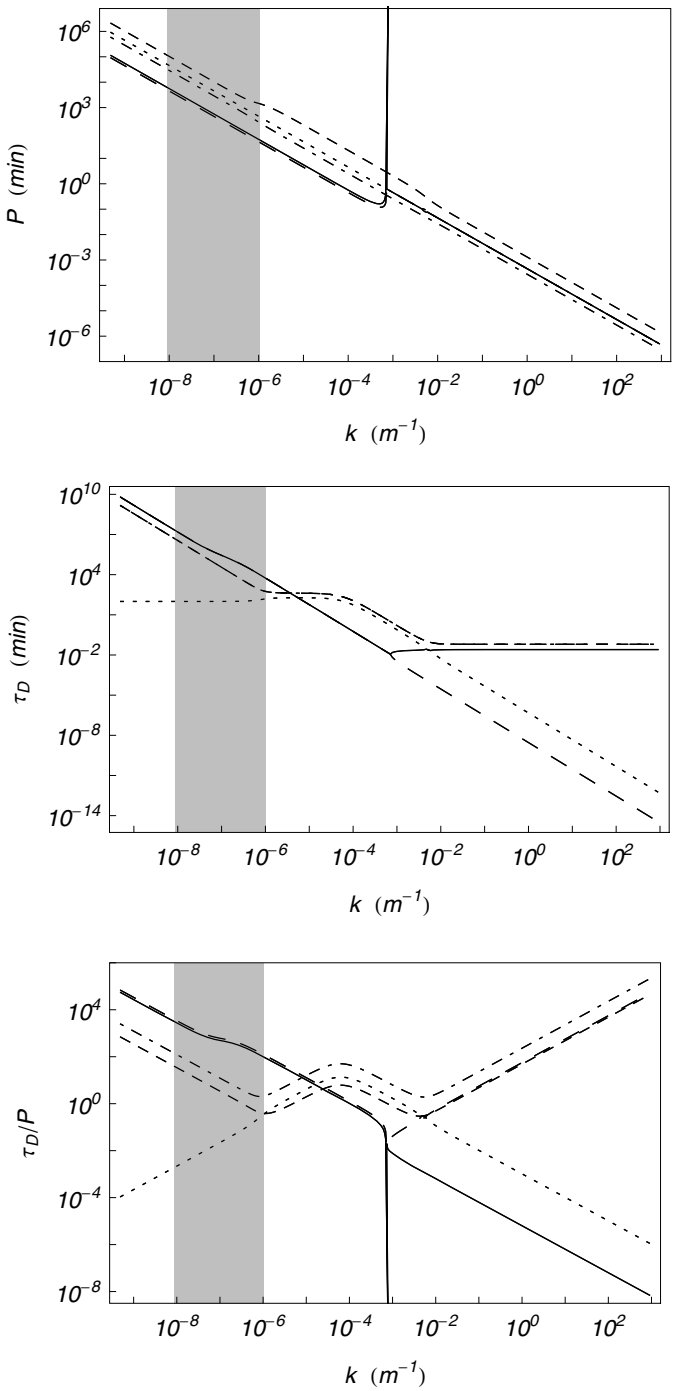

Fig. 7. Period, damping time, and ratio of the damping time to period versus the wavenumber for magnetoacoustic waves in a PIP with $\tilde{\mu} = 0.8$. Slow waves (short-dashed and dot-dashed lines), fast waves (continuous and long-dashed lines), thermal wave (dotted line). The location of the critical wavenumbers is defined by the presence of peaks and bifurcations in the plots. The background flow speed is 15 km s^{-1} and the shaded region corresponds to the interval of observed wavelengths in prominence oscillations.

very similar to those of a FIRP with the exception that the distortion of the curve representing the high-period slow wave is now smaller, probably due to the effect of Cowling's magnetic diffusivity, and that the damping time of fast waves is only slighly distorted, because of non-adiabatic effects, within the region of interest. This suggests that, basically, the behaviour of fast waves is similar to Alfvén waves and that, when non-parallel propagation is considered, the effect of the coupling with slow and thermal waves appears at small wavenumbers. Finally, Fig. 8 displays the behavior of the different waves when the flow speed is decreased to 10 km s^{-1}. It can be seen that at two different wavenumbers the period of the high-period branch of slow waves becomes infinite. The reason is that at these points the flow speed is equal to real part of the non-adiabatic sound speed Λ_r, so the real part

of the slow wave frequency, $\omega_r = k_x(v_0 - \Lambda_r)$, becomes zero. In this sense, Fig. 9 shows the behavior of the real part of the non-adiabatic sound speed, given by Eq. (46), in a flowing and partially ionised plasma, versus the wavenumber k, and we can check that the wavenumbers at which the period become infinite in Fig. 8 correspond approximately to wavenumbers at which $\Lambda_r = 10\ \mathrm{km\,s^{-1}}$.

On the other hand, in this case we can also obtain approximate expressions for the imaginary part of the thermal wave. For small wavenumbers, it is given by Eq. (53), while for large wavenumbers it becomes,

$$\omega_i = \frac{v_a^2 \cos^2\theta (AT_0 - H\rho_0)}{\rho_0 c_s^2 v_a^2 \cos^2\theta + (AT_0 - H\rho_0)\left[\eta_C - \rho_0 v_a^2 \Xi \sin^2\theta\right]}. \quad (74)$$

Now, the ratio of damping time to period is given by Eq. (62) for small wavenumbers, while for large wavenumbers is,

$$\frac{\tau_D}{P} \sim \frac{k_x v_0 \left[c_s^2 v_a^2 \rho_0 \cos^2\theta + (AT_0 - H\rho_0)\eta_C\right]}{2\pi v_a^2 \cos^2\theta (AT_0 - H\rho_0)} + \frac{k_x v_0 \left[(H\rho_0 - AT_0) v_a^2 \Xi \sin^2\theta\right]}{2\pi v_a^2 \cos^2\theta (AT_0 - H\rho_0)}. \quad (75)$$

Both ratios behave as in previous cases and are coincident with the numerical results, in the appropiate range of wavenumbers, such as can be seen in Fig. 7.

5. Effect of magnetic structure

In previous sections, we have studied the free propagation of Alfvén and magnetoacoustic waves in an unbounded medium. However, high-resolution observations have pointed out that filaments are composed of very fine structures, probably magnetic flux tubes, with a typical width in the range 100–600 km and partially filled with flowing cold plasma (Lin et al. 2007).

In order to estimate the effect of such a magnetic structure, slab or cylinder, which would behave as a waveguide of finite width, we set the wavenumber component in the perpendicular direction to magnetic field lines to a fixed value, $k_z L = \pi/2$, with $L = 10^5$ m. Therefore, the propagation angle θ would now depend on k_x in the following way,

$$\theta = \arctan\left(\frac{\pi/2}{k_x L}\right). \quad (76)$$

5.1. Alfvén waves

In this case, the dispersion relation (16) can be written in terms of ω as,

$$\omega^2 - (2k_x v_0 + \mathrm{i}k_x^2\eta_C + \mathrm{i}k_z^2\eta)\omega + k_x^2(v_0^2 - v_a^2) + \mathrm{i}k_x^3\eta_C v_0 + \mathrm{i}k_z^2 v_0 \eta k_x = 0, \quad (77)$$

whose solutions are:

$$\omega_{hfb} = k_x v_0 + \frac{\sqrt{4v_a^2 k_x^2 - (\eta_C k_x^2 + \eta k_z^2)^2}}{2} + \frac{\mathrm{i}(\eta_C k_x^2 + \eta k_z^2)}{2}, \quad (78)$$

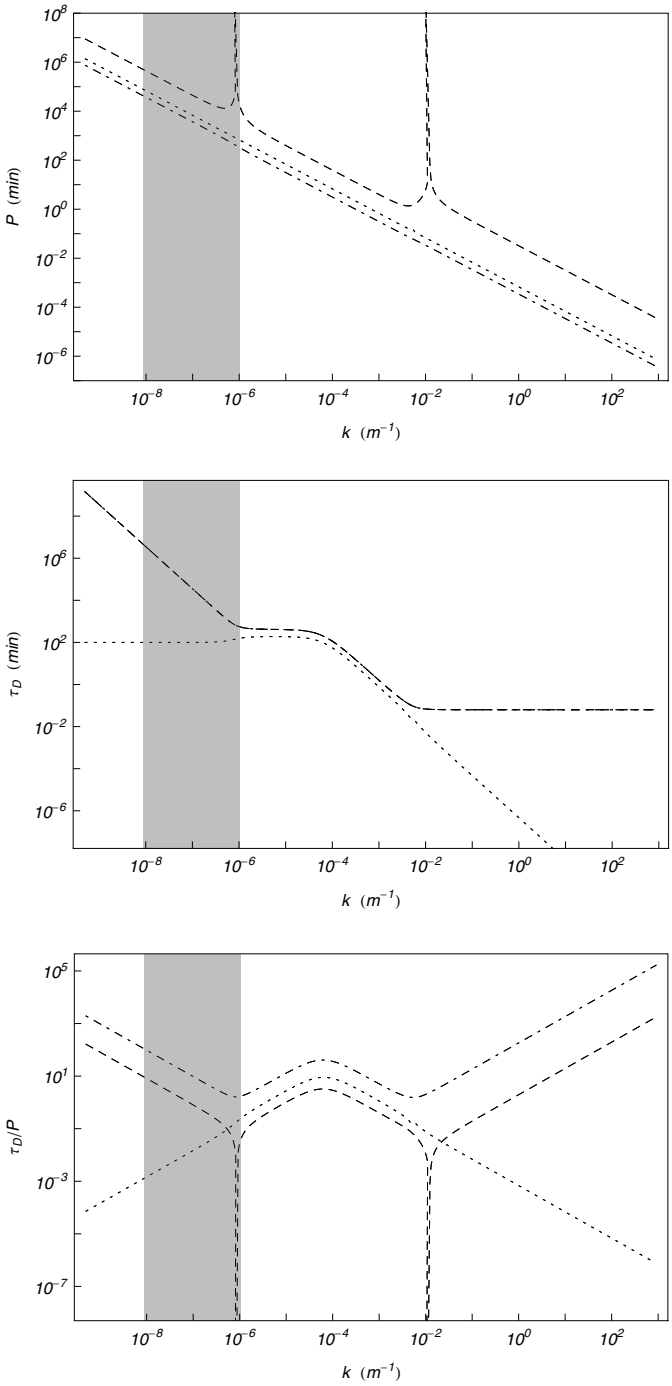

Fig. 8. Period, damping time, and ratio of the damping time to period versus the wavenumber for slow and thermal waves in a PIP with $\tilde{\mu} = 0.8$. Slow waves (short-dashed and dot-dashed lines), thermal wave (dotted line). The background flow speed is 10 km s^{-1} and the shaded region corresponds to the interval of observed wavelengths in prominence oscillations.

and

$$\omega_{lfb} = k_x v_0 - \frac{\sqrt{4v_a^2 k_x^2 - (\eta_C k_x^2 \cos^2 + \eta k_z^2)^2}}{2} + \frac{\mathrm{i}(\eta_C k_x^2 + \eta k_z^2)}{2}. \quad (79)$$

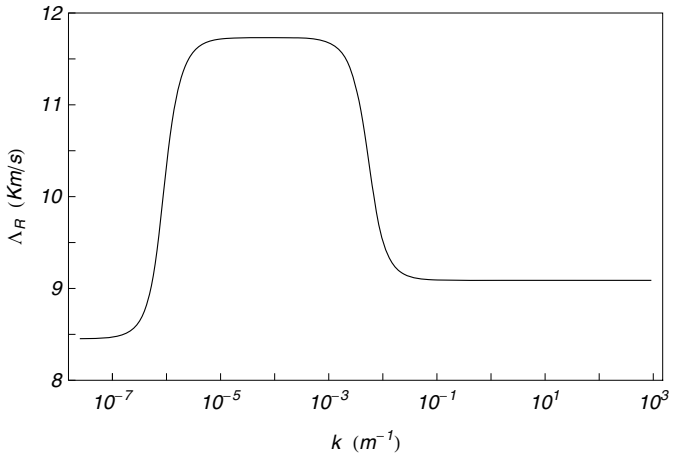

Fig. 9. Real part of the non-adiabatic sound speed, Λ_r, versus the wavenumber. The background flow speed is 10 km s^{-1}.

In this case, the modified Alfvén speed, V_a, becomes,

$$V_a = v_a \sqrt{1 - \frac{(\eta_C k_x^2 + \eta k_z^2)^2}{4 v_a^2 k_x^2}}. \tag{80}$$

Such as in Sect. 3, we could look for the horizontal wavenumber at which the real part of the frequency for the low frequency branch becomes zero, then, imposing that,

$$k_x v_0 - \frac{\sqrt{4 v_a^2 k_x^2 - (\eta_C k_x^2 + \eta k_z^2)^2}}{2} = 0, \tag{81}$$

we obtain a biquadratic equation in k_x such as,

$$k_x^4 + \frac{4(v_0^2 - v_a^2) + 2\eta\eta_C k_z^2}{\eta_C^2} k_x^2 + \frac{\eta^2}{\eta_C^2} k_z^4 = 0, \tag{82}$$

whose solutions are given by,

$$k_x^+ = \pm \sqrt{\frac{A + B}{2}}, \tag{83}$$

and

$$k_x^- = \pm \sqrt{\frac{A - B}{2}}. \tag{84}$$

with

$$A = \frac{4(v_a^2 - v_0^2) - 2\eta\eta_C k_z^2}{\eta_C^2}$$

$$B = \sqrt{\left(\frac{4(v_0^2 - v_a^2) + 2\eta\eta_C k_z^2}{\eta_C^2}\right)^2 - 4\frac{\eta^2}{\eta_C^2} k_z^4}.$$

On the other hand, we could also look for the horizontal wavenumbers at which, for both branches, the square root in Eqs. (78) and (79) becomes zero, i.e. the modified Alfvén speed vanishes. Imposing this condition, we obtain,

$$k_x = \frac{v_a}{\eta_C} \pm \frac{v_a}{\eta_C} \sqrt{\left(1 - \frac{\eta\eta_C k_z^2}{v_a^2}\right)}, \tag{85}$$

so, we are left with four critical horizontal wavenumbers.

Figure 10 displays the above described results for Alfvén waves. We can observe how before arriving to the critical left points both branches have the same period, $2\pi/k_x v_0$, but two different damping times, once the left critical wavenumbers have been attained the periods are different but the damping time is the same and the behavior of both waves is similar to the unbounded case; finally, when the right critical wavenumbers are attained both branches have again the same period, $2\pi/k_x v_0$, but different damping times again. With the help of Eqs. (80), (31) and Fig. 11, we can explain the behavior of the period of the

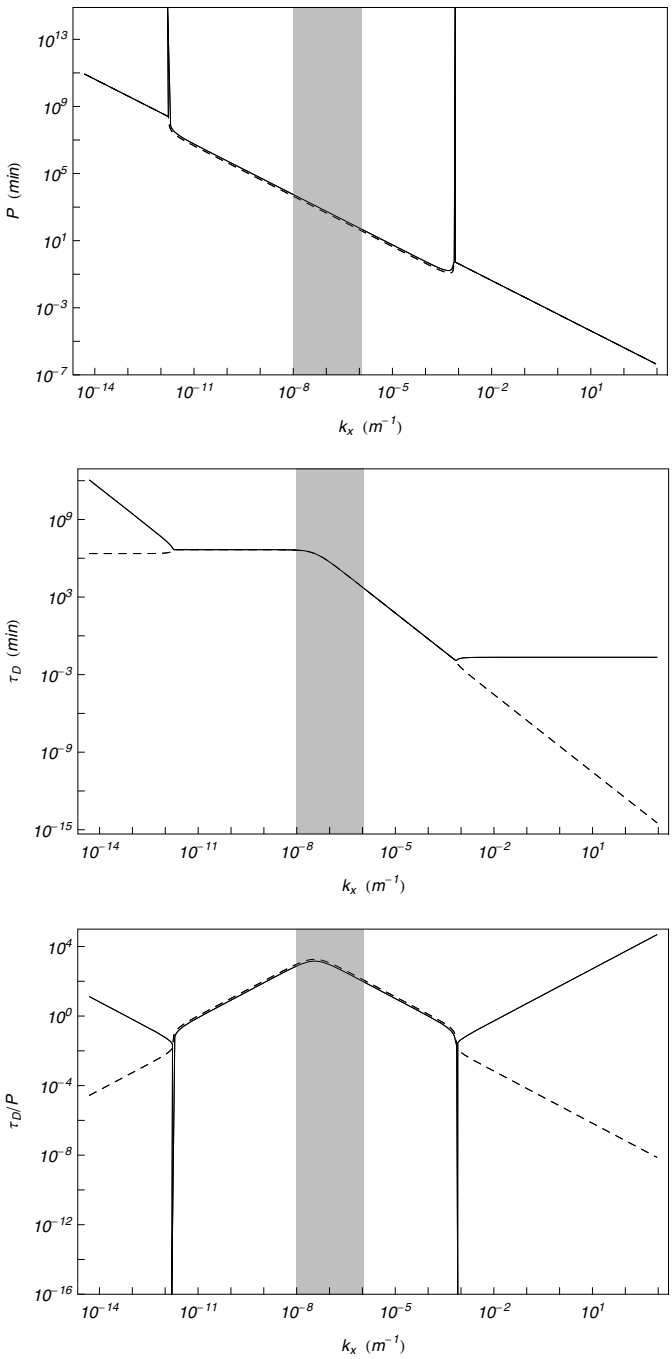

Fig. 10. Period, damping time, and ratio of the damping time to period versus the horizontal wavenumber for the long (solid) and short (dashed) period Alfvén waves in a PIP with $\tilde{\mu} = 0.8$ and $k_z = 1.57 \times 10^{-5}$ m^{-1}. The location of the critical wavenumbers is defined by the presence of peaks and bifurcations in the plots. The background flow speed is 15 km s^{-1} and the shaded region corresponds to an interval of horizontal wavelengths coincident with observed wavelengths in prominence oscillations.

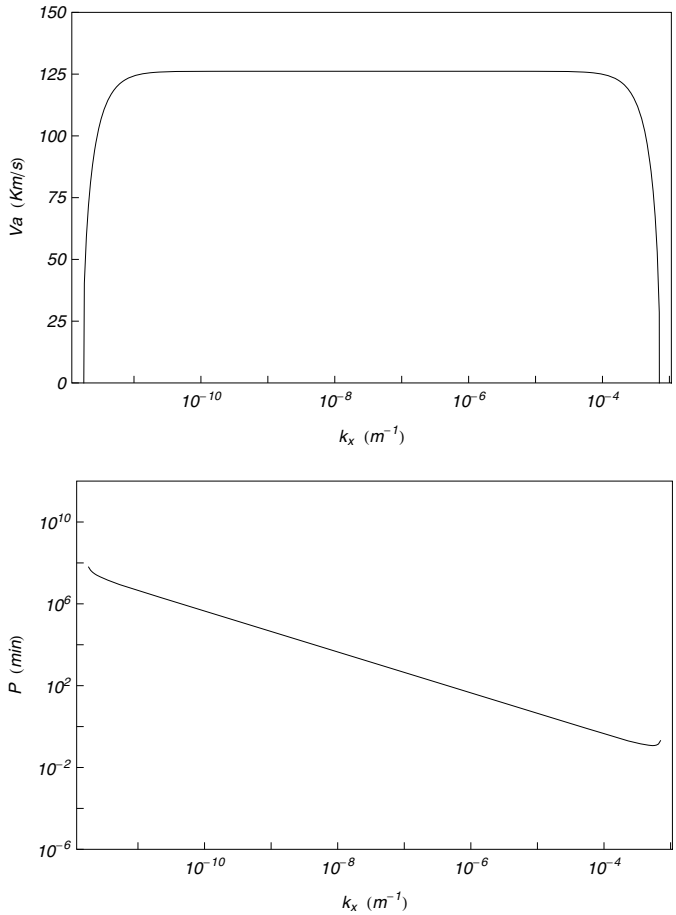

Fig. 11. Modified Alfvén speed (Eq. (80)) and period of the low-period Alfvén wave (Eq. (31)), versus the horizontal wavenumber.

low-period Alfvén wave in this case. Figure 11 displays the behaviors of the modified Alfvén speed and the period of the low-period Alfvén wave computed from Eq. (31), and we can observe that the modified Alfvén speed goes to zero at two different wavenumbers k_x and that the behavior of the period is exactly the same as in Fig. 10, jumping to $2\pi/k_x v_0$ at the two mentioned horizontal wavenumbers.

Furthermore, since for most of the range of the wavenumber k_x the imaginary part of the frequency is basically given by the imaginary parts in Eqs. (78) and (79), when k_x becomes small these imaginary parts become constant which is also reflected in the behavior of the damping time versus k_x in Fig. 10.

Finally, we have considered the maximum thread's width ($L = 6 \times 10^7$ m) reported by observations, and we have computed again the period, damping time and the ratio between the damping time and period. The results show that the left critical points are displaced towards smaller values of the parallel wavenumber, that the behavior of the period does not vary, that the damping time increases by two orders of magnitude for parallel wavenumbers smaller than 10^{-8} m^{-1} and, consequently, that the ratio between both quantities increases in the same order of magnitude for very small parallel wavenumbers. We must keep in mind that to modify thread's width implies to modify the perpendicular wavenumber k_z and, for this reason, the critical parallel wavenumbers obtained from Eqs. (83), (84) and (85) are modified. Regarding the damping time of Alfvén waves in this case, the results shown in Fig. 10 indicate that, again, the damping times are very large as compared to reported observational results and the presence of a magnetic structure does not improve at all the efficiency of the considered damping mechanism.

5.2. Magnetoacoustic waves

The dispersion relation is obtained by modifying Eq. (69) which becomes,

$$\begin{aligned}
\Omega^5 &- \frac{\mathrm{i}\Big(AT_0 + (k_x^2 + k_z^2)p_0\eta_{\mathrm{C}}\Big)}{p_0}\Omega^4 \\
&- \frac{(k_x^2 + k_z^2)[p_0(c_{\mathrm{s}}^2 + v_{\mathrm{a}}^2) + AT_0\eta_{\mathrm{C}}]}{p_0}\Omega^3 \\
&+ \frac{1}{p_0\rho_0}\mathrm{i}(k_x^2 + k_z^2)\Big[AT_0(p_0 + v_{\mathrm{a}}^2\rho_0) \\
&+ p_0\rho_0\Big(c_{\mathrm{s}}^2(k_x^2 + k_z^2)\eta_{\mathrm{C}} - H - c_{\mathrm{s}}^2 v_{\mathrm{a}}^2 k_z^2 \Xi\rho_0\Big)\Big]\Omega^2 \\
&+ \frac{1}{\rho_0}(k_x^2 + k_z^2)\Big[\rho_0\Big(c_{\mathrm{s}}^2 k_x^2 v_{\mathrm{a}}^2 - H(k_x^2 + k_z^2)\eta_{\mathrm{C}} + Hk_z^2 v_{\mathrm{a}}^2\Xi\rho_0\Big) \\
&+ AT_0\Big(k_x^2\eta_{\mathrm{C}} + k_z^2(\eta_{\mathrm{C}} - v_{\mathrm{a}}^2\Xi\rho_0)\Big)\Big]\Omega \\
&+ \frac{\mathrm{i}k_x^2(k_x^2 + k_z^2)v_{\mathrm{a}}^2(H\rho_0 - AT_0)}{\rho_0} = 0. \qquad (86)
\end{aligned}$$

Then, expanding this expression in terms of ω and solving for the fixed k_z, we could obtain the behavior of magnetoacoustic waves. Figure 12 displays the period, damping time and the ratio of damping time to period versus the wavenumber for magnetoacoustic and thermal waves obtained from Eq. (86). We can observe that two critical wavenumbers appear for fast waves but also that one critical wavenumber appears for slow waves. The critical wavenumbers for fast waves are the same that were obtained in the unbounded case but an interesting feature is that the period, damping time and the ratio between damping time and period become constant when going to small wavenumbers. This behavior of the period can be understood in the following way: In a first approximation, the real part of the frequency of fast waves is given by,

$$\omega_{\mathrm{r}} = \sqrt{k_x^2 + k_z^2}(v_0 \pm V_{\mathrm{a}}), \qquad (87)$$

with V_{a} given by Eq. (80). Taking the limit of k_x going to zero in (80) and (87) we obtain,

$$\omega_{\mathrm{r}} = k_z(v_0 \pm v_{\mathrm{a}}), \qquad (88)$$

since V_{a} becomes the usual and constant Alfvén speed v_{a}. Therefore, since k_z is a constant, the period also becomes constant for small k_x and its behavior is quite different when compared with Alfvén waves.

Regarding the behavior of the damping time for fast waves, if we assume that the imaginary part of the frequency is basically given by the imaginary parts in Eqs. (78) and (79), when k_x becomes negligible the behavior of the damping time for fast waves (Fig. 12) should be similar to that one of Alfvén waves (Fig. 10) except that the left bifurcation is missing. Related with the damping time and the damping ratio of fast waves an interesting feature appears which is that within the range of wavelengths of interest the ratio of the damping time to the period is substantially improved as compared with the fully unbounded case. This ratio is around 100 produced by periods of the order of minutes and damping times of the order of 100 minutes.

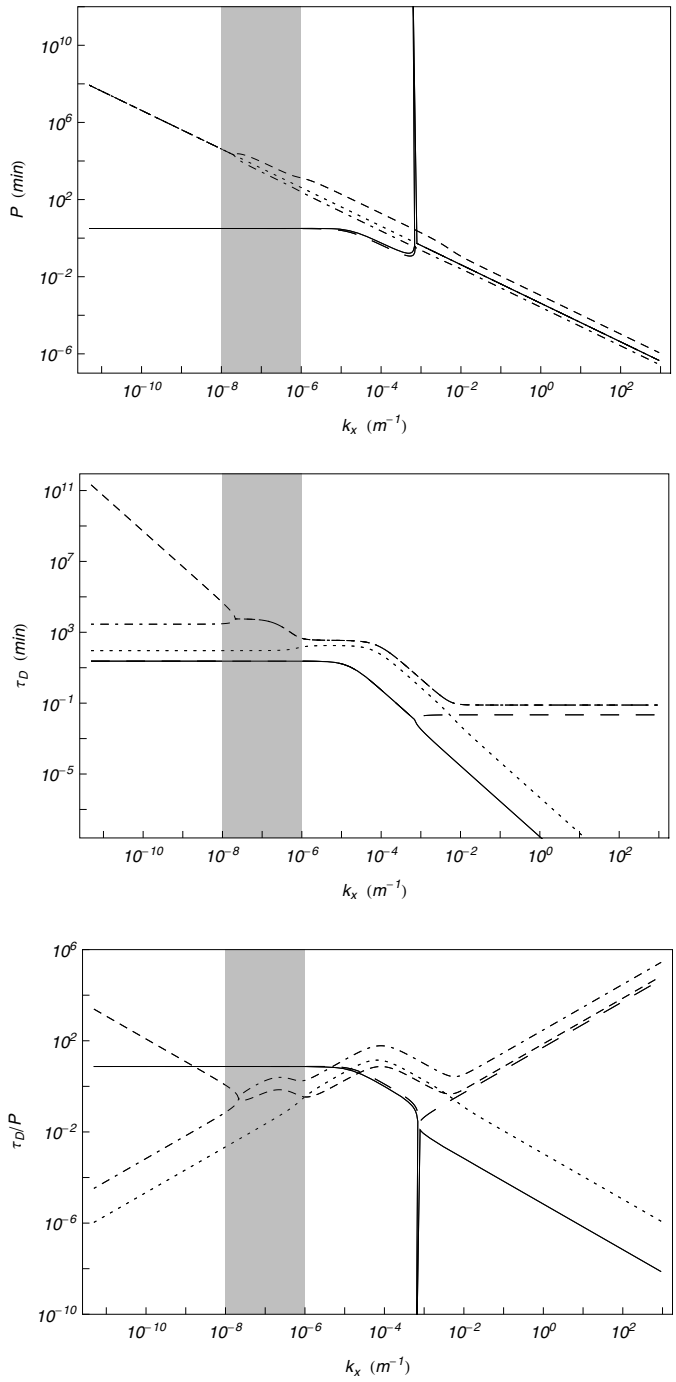

Fig. 12. Period, damping time, and ratio of the damping time to period versus the horizontal wavenumber for magnetoacoustic waves in a PIP with $\tilde{\mu} = 0.8$ and $k_z = 1.57 \times 10^{-5}$ m^{-1}. Slow waves (short-dashed and dot-dashed lines), fast waves (continuous and long-dashed lines), thermal wave (dotted line). The location of the critical wavenumbers is defined by the presence of peaks and bifurcations in the plots. The background flow speed is 15 km s^{-1} and the shaded region corresponds to an interval of horizontal wavelengths coincident with observed wavelengths in prominence oscillations.

Considering now the slow wave, and taking into account Eq. (86), it is quite difficult to obtain an analytic expression for the critical wavenumber. The critical wavenumber occurs at small k_x which suggests that terms of high degree in ω (ω^5, ω^4 and ω^3) could be neglected, but even in this case the remaining expression is too complicate. A different approach could be to compare the value of our critical wavenumber to that obtained by Soler et al. (2009c) in the case of a magnetic cylinder filled with non-flowing, adiabatic and partially ionised plasma. Following Soler et al. (2009c), the expression for the slow wave critical wavenumber, $k_x^{\rm cs}$, is,

$$k_x^{\rm cs} \approx \frac{k_z^2 c_{\rm s} \eta_{\rm C}}{2 v_{\rm a}^2}, \tag{89}$$

which in our case gives $k_x^{\rm cs} = 3.16 \times 10^{-8}$ m^{-1} quite close to the numerical value obtained from our numerical solution shown in Fig. 12. Therefore, we can conclude that the critical wavenumber for the slow wave is practically independent of the non-adiabatic effects and the flow, and is determined, basically, by Cowling's magnetic diffusivity i. e. by the ionisation degree. On the other hand, and taking into account that $\omega = \Omega + k_x v_0$, what happens at the slow wave critical wavenumber is that the real part of the frequency Ω, probably depending on k_x, becomes zero for $k_x^{\rm cs}$ and, then, the real part of the frequency ω for both slow waves becomes $k_x v_0$. For k_x smaller than $k_x^{\rm cs}$, the real part of the frequency $\omega_{\rm r}$ is given by $k_x v_0$, exactly the same as for the thermal wave, while two different imaginary parts appear. On the other hand, for a large range of horizontal wavenumbers the behavior of the imaginary part of the frequency, and so the behavior of the damping time, is dominated by non-adiabatic effects such as in the unbounded case.

Finally, for slow waves, and within part of the region of interest, the ratio of the damping time to period becomes very small and fully compatible with observations, while the behavior of the thermal mode is not modified at all by the effect of magnetic structure.

Finally, we have considered, again, the maximum thread's width ($L = 6 \times 10^7$ m) and computed the period, damping time and the ratio between the damping time and period for fast and slow waves. In the case of slow waves, the results show that the critical point is displaced towards smaller values of the parallel wavenumber, that the behavior of the period does not vary, that the damping time increases by two orders of magnitude for parallel wavenumbers smaller than 10^{-8} m^{-1} and, consequently, that the ratio between both quantities increases in the same order of magnitude for very small parallel wavenumbers. This displacement of the critical wavenumber can be understood by considering Eq. (89) since when L is increased, the value of the perpendicular wavenumber k_z decreases, so, the value of the critical parallel wavenumber also decreases.

In summary, the above results for Alfvén and magnetoacoustic waves provide with a rough information about the effects to be expected when a bounded magnetic structure, containing a flowing, non-adiabatic and partially ionised plasma, is considered. In spite of using this rough approximation to model the presence of a magnetic structure, our results for fast and Alfvén waves are quite similar to those obtained by Soler et al. (2009d) when analysed Alfvén and fast waves in a magnetic cylinder filled with non-flowing, adiabatic and partially ionised plasma, with the difference that only two critical wavenumbers appear in that case.

6. Summary

Solar prominences are composed of partially ionised plasmas which often display time damped small-amplitude oscillations together with flows. Commonly, these oscillations have been interpreted in terms of MHD waves, and different damping mechanisms (thermal, resonant absorption, ion-neutral collisions) have

been proposed. With the aim to analyse the time damping of non-adiabatic MHD waves in a partially ionised prominence-like plasma, we consider a simple configuration consisting of an unbounded prominence medium, permeated by a horizontal magnetic field, and with a background field-aligned flow. The physical properties of the medium are similar to those usually assumed for quiescent prominences.

As it is well known, Alfvén waves are weakly damped by non-adiabatic effects. However, when a partially ionised plasma is considered damping effects due to Cowling's and Spitzer's resistivities appear. In the studied configuration, Alfvén waves are decoupled from magnetoacoustic waves and the above resistive effects are responsible for its damping. Once the dispersion relation for Alfvén waves has been obtained, it can be solved analytically and several interesting features appear. First of all, a critical wavenumber, k_c, similar to that one found in unflowing partially ionised plasmas is also present. In absence of flow, the period of both Alfvén waves becomes infinite at this wavenumber. However, when a flow is present, the period of the low-period branch of Alfvén waves becomes equal to $2\pi/k_x v_0$ at this wavenumber, and keeps the same value for larger wavenumbers. In addition, the presence of flow induces the apparition of a second critical wavenumber, $k_{\rm lfb}$, at which the period of the high-period branch of Alfvén waves becomes infinite; next, for values of the wavenumber between $k_{\rm lfb}$ and k_c, the period of this branch becomes again finite, and when k_c is attained the period becomes also equal to $2\pi/k_x v_0$. Another interesting feature is the behavior of the damping time which is dominated by resistive effects along all the interval of considered wavenumbers. For values of the wavenumber smaller than k_c, only one and the same damping time appears for both branches, however, for wavenumbers larger than k_c two different damping times appear, one is almost constant and independent of the wavenumber while the other decreases in a continuous way, so we are left with two propagating waves, in the same direction, but with different damping times. On the other hand, a modified Alfvén speed, V_a, can be defined, which includes the effect of both resistivities, depends on the wavenumber, k, and tends to the usual Alfvén speed, v_a, for small wavenumbers. When this modified Alfvén speed, or when the combination of this speed and flow speed, are set to zero, we recover the above mentioned critical wavenumbers. The period of Alfvén waves can be written in terms of the flow and modified Alfvén speed and is given by,

$$P = \frac{2\pi}{k\cos\theta(v_0 \pm V_a)},$$

which exactly reproduces the behavior of the period for both branches up to the critical wavenumber k_c. For larger wavenumbers, the period is given by $2\pi/k_x v_0$. In general, and for the physical conditions usually assumed in quiescent prominences, the ratio τ_D/P for Alfvén waves is significantly larger than those usually obtained from observations i. e. in spite of the effect of flow in producing high- and low-period branches, the ratio is almost the same as in the case without flow since the flow speed is always much smaller than the Alfvén speed. Finally, if we consider a FIRP, the behavior of the period is similar to the case of a PIP but the damping time is larger for any value of the wavenumber interval considered. This is so because Spitzer's resistivity is always much smaller than Cowling's resistivity in a PIP, and, therefore, the ratio τ_D/P is very large within the region of interest. A further consequence is that the critical wavenumbers are moved towards larger values. Taking into account these results we can conclude that, in prominence conditions, ion-neutral collisions are not an efficient mechanism for the damping of Alfvén waves, at least within the range of wavelengths of interest.

In the case of non-adiabatic magnetoacoustic waves in a PIP, the obtained dispersion relation couples fast, slow and thermal waves. This dispersion relation is a fifth degree polynomial in the frequency providing with two fast, two slow and one thermal wave. However, if we only consider FIRP and longitudinal propagation then fast waves, now Alfvén waves, decouple from slow and thermal waves which remain coupled. In this case, slow and thermal waves are not affected by resistivity and, for small and large wavenumbers, analytical approximations for the real and imaginary parts of its frequencies can be obtained. For non-parallel propagation the full dispersion relation for a FIRP needs to be solved numerically. The behavior of the period of fast waves is basically similar to that of Alfvén waves and, again, two critical wavenumbers appear. The period of slow waves shows two clearly separated branches, because the flow speed is close to the non-adiabatic sound speed in a flowing and FIRP plasma, and the thermal wave is now a propagating wave whose period is given by $2\pi/k_x v_0$. Regarding the damping mechanisms, fast waves are basically attenuated by resistive effects except for very small wavenumbers when non-adiabatic effects show some influence. Slow waves are damped by non-adiabatic effects as well as the thermal wave whose damping is very strong. The ratio τ_D/P for fast waves is very large within the region of wavelengths of interest, so, the considered damping mechanism is inefficient. For slow waves, the order of magnitude of the ratio is compatible with observations within part of the region of interest, however, this ratio corresponds to the particular case of long period oscillations having large damping times which are not often observed. For the thermal wave, this ratio is very small.

When a PIP is considered the same behaviour as before can be found for the different waves, with the difference that now the critical wavenumbers for fast waves are displaced towards small wavenumbers which is due to the presence of Cowling's resistivity. Although the numerical value of flow speed has been taken within the range of commonly detected values in prominence observations, we could consider to change the flow speed numerical value and study the effect produced by this modification. Decreasing the flow speed to 10 km s^{-1} produces that at two additional wavenumbers the period of the high-period branch of slow waves attains an infinite value, which is a due to the coincidence between the numerical values of flow speed and the real part of the non-adiabatic sound speed. Since the non-adiabatic sound speed is determined by plasma physical conditions, these conditions become of paramount importance.

Another important parameter in the above summarised calculations is the ionisation fraction $\tilde{\mu}$. Varying this parameter, going from an almost fully ionised to an almost neutral prominence, the main effects appear in fast and Alfvén waves since they are influenced by Cowling's resistivity which depends on the ionisation fraction. The modification of Cowling's resistivity modifies the location of critical wavenumbers appearing in fast and Alfvén waves.

Finally, since filaments seem to be composed of very fine structures, probably magnetic flux tubes filled at least partially with cool plasma, we could try to extract some information about the behavior of waves versus the horizontal wavenumber k_x, when the vertical wavenumber k_z is kept constant. First of all, the dispersion relations must be written again and a new modified Alfvén speed can be defined. In the case of Alfvén waves, four critical wavenumbers appear now which can be explained by studying the behavior of the modified Alfvén speed with

respect to the horizontal wavenumber, however, this rough introduction of a magnetic structure worsens the damping time of Alfvén waves within the range of wavelengths of interest. In the case of fast waves things are different, they kept the two already known critical wavenumbers but the period and damping time become constant when going to small horizontal wavenumbers. In particular, this happens within the range of observed wavelengths and gives place to a ratio of the damping time to the period of the order of 100. This ratio is caused by short periods of the order of minutes and damping times of the order of hundreds of minutes i.e. constrained propagation substantially improves the damping ratio for fast waves within the region of interest. The slow wave displays now a critical wavenumber at which its period becomes $2\pi/k_x v_0$ equal to that of the thermal wave. This critical wavenumber appears within the region of interest and produces, for both slow waves, a ratio τ_D/P compatible with observations, but corresponding to long period oscillations having large damping times.

In summary, our results suggest that in flowing partially ionised prominence plasmas, and within the range of observed wavelengths in prominence oscillations, resistive effects, dominated by Cowling's resistivity, are not enough efficient to damp MHD waves responsible for these oscillations. This was already pointed out by Ballai (2003) in unflowing fully ionised prominence plasmas. However, the efficiency of ion-neutral collisions could be improved if the commonly assumed values for the characteristic prominence parameters (density, magnetic field, ionisation fraction) were different (Kuckein et al. 2009; Ju Jing et al. 2010) and as a result the numerical value of Cowling's resistivity is increased. This points out the need of an accurate and proper determination of these characteristic magnitudes. On the other hand, we would like remark that, taking into account the entanglement of the different effects, further information such as polarisation of motions, behavior of perturbations and its relationship with spectroscopic parameters (line width, line intensity), etc. should be needed in order to help us to properly identify the kind of waves responsible for the observed time damped prominence oscillations.

Acknowledgements. Comments from I. Arregui, R. Oliver and R. Soler are gratefully acknowledged. The authors acknowledge the financial support provided by MICINN and FEDER funds under grant AYA2006-07637.

References

Arregui, I., & Ballester, J. L. 2010, Space Sci. Rev., accepted [arXiv:1002.3489]
Arregui, I., Terradas, J., Oliver, R., & Ballester, J. L. 2008, ApJ, 682, L141
Ballai, I. 2003, A&A, 410, L17
Ballester, J. L. 2010, Adv. Space Res., 46, 364
Banerjee, D., Erdélyi, R., Oliver, R., & O'Shea, E. 2007, Sol. Phys., 246, 3
Berger, T. E., Shine, R. A., Slater, G. L., et al. 2008, ApJ, 676, L89
Braginskii, S. I. 1965, Rev. Plasma Phys., 1, 205
Balsara, D. S. 1996, ApJ, 465, 775
Carbonell, M., Oliver, R., & Ballester, J. L. 2004, A&A, 415, 739
Carbonell, M., Terradas, J., Oliver, R., & Ballester, J. L. 2006, A&A, 460, 573
Carbonell, M., Oliver, R., & Ballester, J. L. 2009, New A,14, 277
Chae, J., Park, Y. D., & Park, H. M. 2006, Sol. Phys., 234,115
Chae, J., Ahn, K., Lim, E. K., Choe, G. S., Sakurai, T. 2008, ApJ, 689, L73
Chandrasekhar, S. 1961, Hydrdodynamic and Hydromagnetic stability (Oxford: International Series of Monographs on Physics)
De Pontieu, B., Martens, P. C. H., & Hudson, H. S. 2001, ApJ, 558, 859
Ferraro, V. C. A., & Plumpton, C. 1961, An Introduction to magneto-fluid mechanics (Oxford University Press)
Forteza, P., Oliver, R., Ballester, J. L., & Khodachenko, M. L. 2007, A&A, 461, 731
Forteza, P., Oliver, R., & Ballester, J. L. 2008, A&A, 492, 223
Gilbert, H. R., Hansteen, V. H., & Holzer, T. E. 2002, A&A, 577, 464
Gilbert, H., Kilper, G., & Alexander, D. 2007, ApJ, 671, 978
Goedbloed, H. & Poedts, S. 2004, Principles of Magnetohydrodynamics (Cambridge University Press)
Jess, D. B., Mathioudakis, M., Erdélyi, R., Crockett, P. J., Keenan, F. P. & Christian, D. J. 2009, Science, 323, 1582
Ju Jing, Yuan Yuan, Wiegelman, T., Yan Xu, Rui Liu & Haiming Wan, 2010, ApJ, 719, L56
Kendall, D. C., & Plumpton, C. 1964, Magnetohydrodynamics with Hydrodynamics (Pergamon Press)
Khodachenko, M. L., Arber, T. D., Rucker, H. O., & Hanslmeier, A. 2004, A&A, 422, 1073
Kulsrud, R., & Pearce, W. P. 1969, ApJ, 156, 445
Kuckein, C., Centeno, R., Martínez Pillet, V., et al. 2009, A&A, 501, 1113
Labrosse, N., Heinzel, P., Vial, J. V., et al. 2010, Space Sci. Rev., 151, 243
Landman, D. A., Edberg, S. J., & Laney, C. D. 1977, ApJ, 218, 888
Leake, J. E., Arber, T. D., & Khodachenko, M. L. 2005, A&A, 442, 1091
Lin, Y. 2004, Ph.D. Thesis. University of Oslo (Norway)
Lin, Y., Engvold, O., & Wiik, J. E. 2003, Sol. Phys., 216, 109
Lin, Y., Engvold, O., Rouppe van der Voort, L., Wiik, J. E., & Berger, T. E. 2005, Sol. Phys., 226, 239
Lin, Y., Engvold, O., Rouppe van der Voort, L. H. M., & van Noort, M. 2007, Sol. Phys., 246, 65
Mackay, D., Karpen, J., Ballester, J. L., Schmieder, B., & Aulanier, G. 2009, Space Sci. Rev., 151, 333
Mashnich, G. P., Bashkirtsev, V. S., & Khlystova, A. I. 2009, Astron. Lett., 35, 253
Mercier, C., & Heyvaerts, J. 1977, A&A, 61, 685
Molowny-Horas, R., Wiehr, E., Balthasar, H., Oliver, R., & Ballester, J. L. 1999, JOSO Ann. Rep., 126
Ning, Z., Cao, W., Okamoto, T. J., Ichimoto, K., & Qu, Z. Q. 2009a, A&A, 499, 595
Ning, Z., Cao, W., & Goode, P. R. 2009b, ApJ, 707,1124
Okamoto, T. J., et al. 2007, Science, 318, 1557
Oliver, R. 2009, Space Sci. Rev., 149, 175
Oliver, R., & Ballester, J. L. 2002, Sol. Phys., 206, 45
Patsourakos, S., & Vial, J.-C. 2002, Sol. Phys., 208, 253
Schmieder, B., Bommier, V., Kitai, R., et al. 2008, Sol. Phys., 247, 321
Schmieder, B., Chandra, R., Berlicki, A., & Mein, P. 2010, A&A, 514, A68
Singh, K. A. P., & Krishan, V. 2009, New A, 15, 119
Soler, R. 2010, Ph.D. Thesis, Universitat Illes Balears
Soler, R., Oliver, R., & Ballester, J. L. 2007, A&A, 471, 1023
Soler, R., Oliver, R., & Ballester, J. L. 2008, ApJ, 684, 725
Soler, R., Oliver, R., & Ballester, J. L. 2009a, ApJ, 693, 1601
Soler, R., Oliver, R., & Ballester, J. L. 2009b, ApJ, 695, L166
Soler, R., Oliver, R., & Ballester, J. L. 2009c, New A, 14, 238
Soler, R., Oliver, R., & Ballester, J. L. 2009d, ApJ, 699, 1553
Soler, R., Oliver, R., & Ballester, J. L. 2009e, ApJ, 707, 602
Soler, R., Oliver, R., & Ballester, J. L. 2010, A&A, 512, A28
Tanenbaum, B. S. 1961, Phys. Fluids, 4, 1262
Tanenbaum, B. S., & Mintzer, D. 1962, Phys. Fluids, 5, 1226
Terradas, J., Molowny-Horas, R., Wiehr, E., et al. 2002, A&A, 393, 637
Terradas, J., Carbonell, M., Oliver, R., & Ballester, J. L. 2005, A&A, 434, 741
Tsubaki, T. 1988, Solar and Stellar Coronal Structures (National Solar Observatory)
Tsubaki, T., & Takeuchi, A. 1986, Sol. Phys., 104, 313
Watanabe, T. 1961a, Can. J. Phys., 39, 1044
Watanabe, T. 1961b, Can. J. Phys., 39, 1197
Watts, C., & Hanna, J. 2004, Phys. Plasmas, 11, 1358
Wiehr, E., Balthasar, H., & Stellmacher, G. 1989, Hvar Obs. Bull. 13, 131
Woods, L. C. 1962, J. Fluid Mechanics, 13, 570
Zirker, J. B., Engvold, O., & Martin, S. F. 1998, Nature, 434, 741